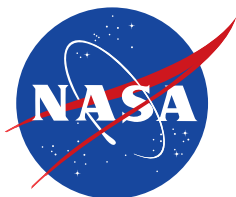


NASA/CR-2004-210725



# **A Six-Node Curved Triangular Element and a Four-Node Quadrilateral Element for Analysis of Laminated Composite Aerospace Structures**

*C. Wayne Martin and David M. Breiner  
Martin Engineering Inc.  
Lincoln, Nebraska*

*Under NASA Contracts NAS4-97007,  
NAS4-50079, NCA2-318, and NCA2-497*

---

**July 2004**

## The NASA STI Program Office...in Profile

Since its founding, NASA has been dedicated to the advancement of aeronautics and space science. The NASA Scientific and Technical Information (STI) Program Office plays a key part in helping NASA maintain this important role.

The NASA STI Program Office is operated by Langley Research Center, the lead center for NASA's scientific and technical information. The NASA STI Program Office provides access to the NASA STI Database, the largest collection of aeronautical and space science STI in the world. The Program Office is also NASA's institutional mechanism for disseminating the results of its research and development activities. These results are published by NASA in the NASA STI Report Series, which includes the following report types:

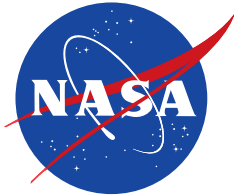
- **TECHNICAL PUBLICATION.** Reports of completed research or a major significant phase of research that present the results of NASA programs and include extensive data or theoretical analysis. Includes compilations of significant scientific and technical data and information deemed to be of continuing reference value. NASA's counterpart of peer-reviewed formal professional papers but has less stringent limitations on manuscript length and extent of graphic presentations.
- **TECHNICAL MEMORANDUM.** Scientific and technical findings that are preliminary or of specialized interest, e.g., quick release reports, working papers, and bibliographies that contain minimal annotation. Does not contain extensive analysis.
- **CONTRACTOR REPORT.** Scientific and technical findings by NASA-sponsored contractors and grantees.
- **CONFERENCE PUBLICATION.** Collected papers from scientific and technical conferences, symposia, seminars, or other meetings sponsored or cosponsored by NASA.
- **SPECIAL PUBLICATION.** Scientific, technical, or historical information from NASA programs, projects, and missions, often concerned with subjects having substantial public interest.
- **TECHNICAL TRANSLATION.** English-language translations of foreign scientific and technical material pertinent to NASA's mission.

Specialized services that complement the STI Program Office's diverse offerings include creating custom thesauri, building customized databases, organizing and publishing research results...even providing videos.

For more information about the NASA STI Program Office, see the following:

- Access the NASA STI Program Home Page at <http://www.sti.nasa.gov>
- E-mail your question via the Internet to [help@sti.nasa.gov](mailto:help@sti.nasa.gov)
- Fax your question to the NASA Access Help Desk at (301) 621-0134
- Telephone the NASA Access Help Desk at (301) 621-0390
- Write to:  
NASA Access Help Desk  
NASA Center for AeroSpace Information  
7121 Standard Drive  
Hanover, MD 21076-1320

NASA/CR-2004-210725



# **A Six-Node Curved Triangular Element and a Four-Node Quadrilateral Element for Analysis of Laminated Composite Aerospace Structures**

*C. Wayne Martin and David M. Breiner  
Martin Engineering Inc.  
Lincoln, Nebraska*

*Prepared for  
NASA Dryden Flight Research Center  
Edwards, California  
Under NASA Contracts NAS4-97007,  
NAS4-50079, NCA2-318, and NCA2-497*

National Aeronautics and  
Space Administration

Dryden Flight Research Center  
Edwards, California 93523-0273

---

**July 2004**

## NOTICE

Use of trade names or names of manufacturers in this document does not constitute an official endorsement of such products or manufacturers, either expressed or implied, by the National Aeronautics and Space Administration.

Available from the following:

NASA Center for AeroSpace Information (CASI)  
7121 Standard Drive  
Hanover, MD 21076-1320  
(301) 621-0390

National Technical Information Service (NTIS)  
5285 Port Royal Road  
Springfield, VA 22161-2171  
(703) 487-4650

# CONTENTS

	<u>Page</u>
SUMMARY.....	1
INTRODUCTION.....	1
ELEMENT PERFORMANCE .....	2
MATHEMATICAL DEVELOPMENT .....	4
CONCLUDING REMARKS.....	7
REFERENCES .....	8
ACKNOWLEDGEMENT.....	9
APPENDIX A: CURVED ELEMENT DEVELOPMENT.....	19
APPENDIX B: MODIFICATIONS TO $B_0$ .....	27
APPENDIX C: SHEAR PERPENDICULAR TO SURFACE IN FLAT ELEMENTS .....	28
APPENDIX D: STRAIN CALCULATION AT NODES.....	36
APPENDIX E: OUT-OF-PLANE ROTATION STIFFNESS .....	39
APPENDIX F: SIMULATED ANTI-SYMMETRIC BENDING MODE .....	42
APPENDIX G: 6-NODE FLAT SHEAR PANEL (USING 10 NODE SHAPE FUNCTIONS). .	45

## TABLES

1.NAFEMS LE2 Results .....	10
2.NAFEMS LE3 Results .....	11
3.Scordelis-Lo Roof Results .....	12
4.Morley Skew Plate Result .....	13
5.Plunkette's Vibrating Wedge Results.....	14
6.NAFEMS T1 Results .....	15
7.Results for NAFEMS Laminated Strip.....	16
8(a). NAFEMS LE2 Curved Shell Patch Test 1989 Results .....	17
8(b). NAFEMS LE3 Pinched Hemisphere Shell 1989 Results .....	17
9.Error Summary for 6 and 8 Node Elements on Six Critical Test Cases.....	18

# FIGURES

	<u>Page</u>
1.NAFEMS LE2 .....	10
2.NAFEMS LE3 .....	11
3(a). Scordelis-Lo Roof .....	12
3(b). Scordelis-Lo Roof Results .....	12
4(a). Morley Skew Plate .....	13
4(b). Morley Skew Plate Results .....	13
5.Plunkett's Vibrating Wedge .....	14
6.NAFEMS T1 .....	15
7.NAFEMS Laminating Strip .....	16
C.1. Sign Conventions and Shear Deformation Relations .....	29
(a). Deformation in x-z plane .....	29
(b). Deformation in y-z plane .....	29
(c). Shear deformation without bending .....	29
C.2.Nodal Configurations and Interpolation Terms .....	30
G.1. 10-Node Triangle .....	45

## **SUMMARY**

Mathematical development and some computed results are presented for Mindlin plate and shell elements, suitable for analysis of laminated composite and sandwich structures. These elements use the conventional 3 (plate) or 5 (shell) nodal degrees of freedom, have no communicable mechanisms, have no spurious shear energy (no shear locking), have no spurious membrane energy (no membrane locking) and do not require arbitrary reduction of out-of-plane shear moduli or under-integration. Artificial out-of-plane rotational stiffnesses are added at the element level to avoid convergence problems or singularity due to flat spots in shells.

In regular rectangular meshes, the Martin-Breiner 6-node triangular curved shell (MB6) is about equivalent to the conventional 8-node quadrilateral with 2x2 integration (which is quite good). In distorted meshes, this 6-node triangular element is distinctly better. The accuracy of the MB6 is most evident in the NAFEMS LE2 curved shell patch test, where error at the specified point is only 0.12 percent, and maximum error anywhere in the patch is 2.5 percent. In contrast, results for five 6 and 8 node elements in commercial programs showed errors of 8 percent to 85 percent at the specified point, and maximum errors as large as -99 to +100 percent at some points in the patch. The four-node quadrilateral, MB4, has very good accuracy for a four-node element, and may be preferred in vibration analysis because of narrower bandwidth.

The mathematical developments used in these elements, included here in seven appendices, have been applied to elements with 3, 4, 6, and 10 nodes and can be applied to other nodal configurations.

## **INTRODUCTION**

Since the inception of finite element analysis, efforts have been made to develop accurate shell elements. Many formulations have been tried, and no attempt at review will be made here. Some element formulations are plagued by spurious shear strains ("shear locking"); some by spurious membrane strains ("membrane locking"). Some elements or element options may represent bending deformation well but not membrane deformation. Other elements or element options may represent membrane deformation well but not bending. Few have been equally accurate for all deformation modes. The

unwary analyst may assume that because a given element and mesh solves one load case correctly, it will be equally accurate for a different load case. The eight- node isoparametric shell with 2x2 integration may be quite accurate when rectangular, but it is under-integrated and much less accurate when its shape is distorted.

The six-node curved triangular shell, MB6, presented here is believed to be a significant advancement because it has excellent and uniform accuracy in all deformation modes, and needs no “options” for different load cases, etc. The triangular shape allows easy mesh generation around openings and discontinuities where a rectangular element’s shape must be severely distorted. Accuracy of stresses is most improved where it is most important; in regions of high stress gradients.

The four-node warped quadrilateral shell, MB4, performs very well, and may be preferred for vibration analysis because of its narrower bandwidth. In-plane deformation can be improved by optional inclusion of incompatible modes [4]. Bending deformation can be improved by optional activation of a simulated antisymmetric bending mode.

## **ELEMENT PERFORMANCE**

The National Agency for Finite Element Methods and Standards in the U.K. supported development of testing procedures and test cases for evaluating finite elements and programs, beginning with a set of benchmark problems by Barlow and Davies in 1986 [5]. Four of these NAFEMS test cases are shown in Figures 1,2,6, and 7. In addition, some other popular test cases are shown; the Scordelis-Lo roof [1,2] in Figure 3; the Morley skew plate [6] in Figure 4; and Plunkett’s vibrating wedge [7] in Figure 5. Some results for these test cases are shown in Tables 1 to 7.

Results of NAFEMS tests for some commercial programs were published in Benchmark Magazine in 1989 [8]. Some results for the LE2 and LE3 shell test cases are shown in Table 8. Errors were quite significant, and at least one entry appears over-optimistic.

More recent calculations (February 1999) suggest that some commercial programs still contained shell elements with poor accuracy. Table 9 shows results for 5 important test cases for six-node elements in two versions of NASTRAN, and for the Ahmad-Irons-Zienkiewicz (AIZ) [1] elements which are contained in some popular programs, as well as the MB6. The NAFEMS LE2 test, described in Figure 1, only asks for the stress at the outer surface at point E, and errors in these average stresses are shown in Table 9. Some



stresses at other points in the patch are shown in parentheses. Note that this is a patch test, and stress should be constant everywhere. However, it is possible to get stresses from 99 percent low to about 100 percent high from one of these commercial programs at some points in the patch. Selection of the “best” element option may improve results, but criteria for selecting these options and reasons for which is the default are not necessarily clear. In contrast, the MB6 error in the LE2 test is only 0.12 percent at the specified point, and its maximum error anywhere in the patch for either load case is 2.5 percent. In addition, the default element option in “NASTRAN B” did not converge for either 4 or 6 node elements in the Scordelis-Lo roof [1,2], Figure 3.

The MB6 and MB4 elements perform very well on the critical test cases in Figures 1 to 7.

Some results are presented in tables 1 to 7 from seven of the test cases used in element validation. Elements are identified as follows:

MB10 is the Martin-Breiner 10-node triangular shell

MB6 is the Martin-Breiner 6-node triangular shell

MB4 is the Martin-Breiner 4-node quadrilateral shell

MB4SI is the Martin-Breiner 4-node quadrilateral with simulated antisymmetric bending mode and incompatible in-plane modes active.

AIZ6 is the Ahmad-Irons-Zienkiewicz 6-node triangular shell.

AIZ8 is the Ahmad-Irons-Zienkiewicz 8-node quadrilateral shell.

AIZ10 is the Ahmad-Irons-Zienkiewicz 10-node triangular shell

LU71S is a 3-node triangular shell [3, 10, 16] with the addition of a simulated antisymmetric bending mode (SABM).

In NAFEMS LE2 [5], Figure 1 and Table 1, the stress should be uniform throughout. MB6 is the only element tabulated which has a near-zero error in average stress and near-zero standard deviation in both cases. The MB6 stress is also nearly uniform throughout, whereas for some other elements it is not. The maximum error for the MB6 at any node of any element, either top or bottom surface and either load case is 2.5 percent.

In NAFEMS LE3 [5], Figure 2 and Table 2, the MB6 is much more accurate than the other quadratic elements in the coarse mesh. The LU71S element is surprisingly accurate in the coarse mesh.

In the Scordelis-Lo Roof [1,2], Figure 3 and Table 3, the MB6 has, by far, the fastest convergence. In comparing calculated results, divergence was observed in some other elements/programs at about 16 nodes per side.

In the Morley skew plate, [6], Figure 4 and Table 4, the MB6 has very good accuracy, and other elements shown require many more degrees of freedom to get under 1 percent error.

Plunkett's vibrating wedge [7], Figure 5 and Table 5, is a severe test of performance with variable thickness. The MB6 computed the most (10) mode shapes that corresponded to Plunkett's sketches, whereas the AIZ8 computed only 8. Also, the MB6 errors in frequencies were smaller than the AIZ8 in 5 of those first 8 modes, and smaller than the AIZ6 in 9 of the 10 modes.

In NAFEMS T1 [5], Figure 6 and Table 6, both 6-node shells MB6 and AIZ6 give excellent results, whereas the 8-node shell, AIZ8, is 7.8 percent low. Performance of the 4-node shell, MB4, with incompatible in-plane modes is very good.

In the NAFEMS laminated strip test case, [9] Figure 7 and Table 7, all of the elements compared give very accurate results for deflection and bending stress. The MB6 error in interlaminar stress is 2.4 percent, which is good, although the AIZ element errors are even smaller.

It is expected that the 6-node triangle, MB6, will be a particularly useful element in stress analysis of laminated composite plate and shell structures. It has nearly the same excellent accuracy in all deformation modes, and needs no "options" for different conditions. It needs only 3 integration points, and thus can be computationally efficient. Two triangles could easily be joined to make a 9-node or 8-node quadrilateral with a total of 6 integration points. Triangular elements have obvious advantages in modeling around discontinuities such as openings, joints and reinforcements where stresses are highest and most important.

## **MATHEMATICAL DEVELOPMENT**

The basic formulation of the elements described here follows Ahmad-Irons-Zienkiewicz [1] with some modifications. The basic formulation is reviewed in Appendix A. Note that matrices are generated in element coordinates, with nodes 1,2,3 defining the x-y plane. One significant change is that nodal rotations are interpolated as expressed in Equation A5. It follows that bending strain terms do not include terms with derivatives of thickness, as in Equation A12, since they would produce strains due to rigid body motion.

This change was made to avoid singularity or near singularity in tapered elements with very thin edges, as in Plunkett's vibrating wedge [7]. If only constant thickness elements or elements with modest taper are to be analyzed, this modification is not necessary or even helpful. All of the numerical results presented here were generated by computer code that builds the element matrix layer-by-layer with two integration points through the thickness of each layer. However, it is shown in Equations A17 to A19 that code could be written with explicit integration through the thickness, which should execute faster. Note that only the stretching and bending parts of the stiffness are computed by the process in Appendix A, and an important modification to the membrane strain is described in Appendix B. The out-of-plane shearing stiffness is computed by a different process, shown in Appendix C.

Appendix B shows an important innovation, not previously published, which eliminates spurious membrane strain or "membrane locking". In curved quadratic elements (e.g. the AIZ 6-node triangle and 8-node quadrilateral) bending causes spurious mid-surface strains except at the 2x2 Gauss points. These spurious strains cause serious errors in fully integrated AIZ elements when the "rise" (deviation from flatness) of the element is only about 1/5 of the thickness. A happy exception is the (under-integrated) 8-node rectangular quadrilateral with 2x2 integration, since the spurious strains are correctly zero at the 2x2 Gauss points. However, this is little help in a triangular element or in a quadrilateral whose shape is significantly distorted.

The technique used here to eliminate spurious membrane strain is, in concept, surprisingly simple. It is observed that the average mid surface strain due to constant-moment bending in the element is correct. The correct average strain can be obtained by averaging strains at the integration points. Unfortunately, this eliminates the gradient in mid-surface strains, which is needed for accurate solution of some problems, and it introduces mechanisms.

In the 6-node triangular element, the gradient can be restored by using strains from triangular sub-regions, as shown in Appendix B. It can be shown that this process for recovering the mid surface strain gradient is exact for all constant strain states and all linear strain states in a flat 6-node triangle with straight sides.

This concept probably could be applied to the 8-node quadrilateral with full (3x3) integration, which should make it capable of more distortion in shape. However, a 9-node or 8-node quadrilateral with only 6 total integration points can easily be generated by joining two 6-node triangles, which should be about equally accurate and require less compute time.

Appendix C shows the method for calculating out-of-plane shear strain. This concept originated with Utku [3], who applied it to a 3-node flat shell. The basic concept is that the function used to interpolate out-of-plane

displacement must be one order higher than the function used to interpolate rotations. This eliminates the problem of spurious shear strains (“shear locking”). The concept was applied to laminated composite shells in Reference [10], extended to a 6-node triangle by Yu [11], and generalized to any nodal configuration by Martin and Breiner [12].

The procedure in Appendix C is strictly valid only for flat elements. However, the MB6 matrices are generated in element axis with the x-y plane defined by nodes 1-2-3. If the included angle of the element (angle between outward normals at opposite sides) is 20 degrees, the angle between the outward normal and the z-axis does not exceed 10 degrees. The cosine of 10 degrees is 0.985, so the error is small. This could be considered a limitation of the MB6; that its included angle should not exceed about 20 degrees. However, in the Scordelis-Lo roof [1,2], Figure 3 and Table 3, the MB6 solution is quite accurate with only two elements, which span 40 degrees. More study of this limitation is needed, and the method should be developed for highly curved elements.

Elements that use this procedure have one mechanism, which however is suppressed by joining two elements. The mechanism can be physically described as a relative rotation of top and bottom surfaces about the centroid, with no strain energy. Although deflections are always quite accurate, some imperfections in element strains in the MB6 have been observed in a linear bending problem. Accuracy of strains is improved by using the weighted least squares fit of equation C20 and C21. This may be related to the mechanism, and more study of this may be appropriate.

Appendix D shows the method of calculating strains at nodes used in the new elements.

Appendix E shows the method, not previously published, used in all elements to generate artificial rotational stiffness about the z-axis. This is necessary because these elements inherently have only two rotational stiffness degrees of freedom at each node. The artificial stiffness must be added so that coordinate transformation of the element matrix and assembly with 6 degrees of freedom per node is possible. Selecting these artificial stiffnesses so that they avoid mechanisms, constraints and ill conditioning, but do not significantly stiffen the structure or add strains due to rigid body motion has been a persistent problem.

The method discussed here meets all of the criteria just mentioned. It is a combination of one reported by Zienkiewicz [13] and one due to Kanok Nukulchai [14]. In a flat plate, each of these methods requires fixing at least one out-of-plane rotational degree of freedom to avoid a singularity. Used in combination, there are no mechanisms, and no special attention is needed for calculations such as vibration of a flat free-free plate.

Appendix F shows the development of the simulated antisymmetric bending mode (SABM) which is an option in 3 and 4-node elements. Linear Mindlin elements can express symmetric bending exactly, but are not capable of antisymmetric bending. The SABM substitutes shear deformation for antisymmetric bending deflection with the objective of preserving the correct total strain energy in “beam strips”. The method of Appendix F has proven very effective when applied to the 3-node element [15,16]. When applied to the 4-node element, it is too soft under some conditions, so an arbitrary reduction in the softening effect may be appropriate. Additional study of the application of the SABM to the 4-node element might lead to significant improvement.

## **CONCLUDING REMARKS**

Some techniques for improvement of Mindlin shell elements for analysis of laminated composite aerospace structures, developed with support from several NASA contracts, are brought together in the Appendices of this report. These techniques have been applied to elements with 3, 4, 6, and 10 nodes, and can be applied to other nodal configurations. Performance data for the MB4 4-node quadrilateral and the MB6 6-node triangular elements, which use these techniques, are also presented.

The MB6 6-node triangle has uniformly excellent accuracy in all deformation modes, needs no options for different conditions, and performs much better than elements in some commercial programs in critical test cases. In regular rectangular meshes it is about equivalent to the 8-node quadrilateral with 2x2 integration. In distorted meshes it is distinctly better. The triangular shape is an advantage in modeling. It should be universally adopted for stress analysis of laminated composite aerospace structures.

The LU71 3-node [10, 16] and MB4 4-node elements have proven to be quite effective and robust, particularly in vibration analysis.

## REFERENCES

1. AHMAD, S., IRONS, B.M., and ZIENKIEWICZ, O.C., Analysis of Thick and Thin Shell Structures by Curved Finite Elements. Int. J. Numerical Methods Engrg. Vol. 2, pp. 419-451, 1970.
2. PAWSEY, S.F. and CLOUGH, R.W., Improved Numerical Integration of Thick Shell Finite Elements. Int. J. Numerical Methods Engrg. Vol. 3, pp. 575-586, 1971.
3. UTKU, S. On Derivation of Stiffness Matrices with  $C^0$  Rotation Fields for Plates and Shells. Air Force Third Conference on Matrix Methods in Structural Mechanics. AFFDL-TR-71-160. R.M. Bader et al, Ed., Wright-Patterson AFB, Ohio, 1971.
4. WILSON, E.L., TAYLOR, R.L., DOHERTY, W.P. and GHABOUSSI, J., Incompatible Displacement Models, Numerical and Computer Methods in Structural Mechanics, S.J. Fenves (ed.), Academic Press, 1973.
5. BARLOW, J. and DAVIES, G.A.O., Selected Benchmarks in Structural and Thermal Analysis, National Agency for Finite Element Methods and Standards, Glasgow, 1986.
6. ZIENKIEWICZ, O.C. and ZHU, J.Z., Error Estimates and Adaptivity, Benchmark, July, 1989.
7. PLUNKETT, R., Natural Frequencies of Uniform and Non-uniform Rectangular Cantilever Plates. J. Mechanical Engineering Science, Vol. 5, No.2, 1963.
8. Benchmark Magazine, October 1989 p. 21
9. Benchmark Magazine, March 1994, p. 3
10. Martin, C. W., Lung, S. F., and Gupta, K.K., A Three-Node  $C^0$  Element for Analysis of Laminated Composite Sandwich Shells, NASA TM4125, 1989
11. Yu, H., Performance of a Higher-Order Triangular Finite Element for Composite Laminated Structures. Dissertation presented to the Graduate College, University of Nebraska, Lincoln, Nebraska, December, 1992.
12. Martin, C. W., and Breiner, D. M., Improved Mindlin Plate and Shell Elements. Proceedings of the NAFEMS World Congress 1999 on Effective Engineering Analysis pp. 333-344.
13. Zienkiewics, O. C., and Taylor, R. L. The Finite Element Method Fourth Ed. Vol. 2 McGraw-Hill 1991.

14. Kanock-Nukulchi, W. A., A simple and Efficient Finite Element for General Shell Analysis. Int. J. Num. Meth. Engrg. V 14 No 2 pp. 179-200, 1979.
15. Martin, C. W., Yu, H. and Lung, S. F. Efficient elements for Mindlin Beams and Plates. Proceedings of the Tenth Conference on Electronic Computation. American Society of Civil Engineers, Indianapolis, April 1991 pp. 303-310.
16. Martin, C. W. and Lung S. F., A Three-Node  $C^0$  Mindlin Plate and Shell Element with Simulated Antisymmetric Bending Mode, pp. 327-332 in Advances in Computational Engineering Science, S. N. Atluri and G. Yagawa Ed. Tech Science Press, 1997.

#### **ACKNOWLEDGEMENT**

This work was supported by several NASA contracts through Dryden Flight Research Center, and partially included in contract reports NAS4-97007, December 1998; NAS4-50079, June 1996; NCA2-318, May 1990; and NCA2-497 April 1991.



# NAFEMS LE2 [5] RESULTS

Target Stress at E = 60.0 MPa for both Cases

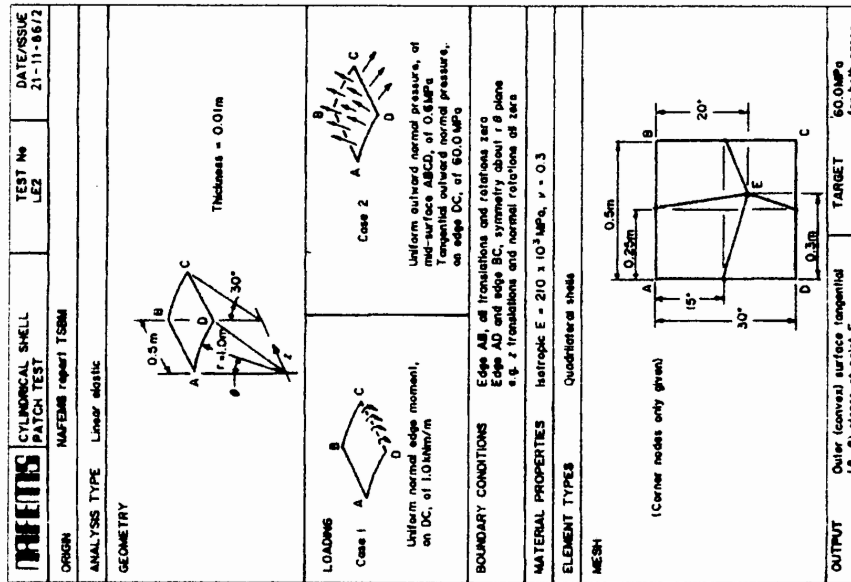
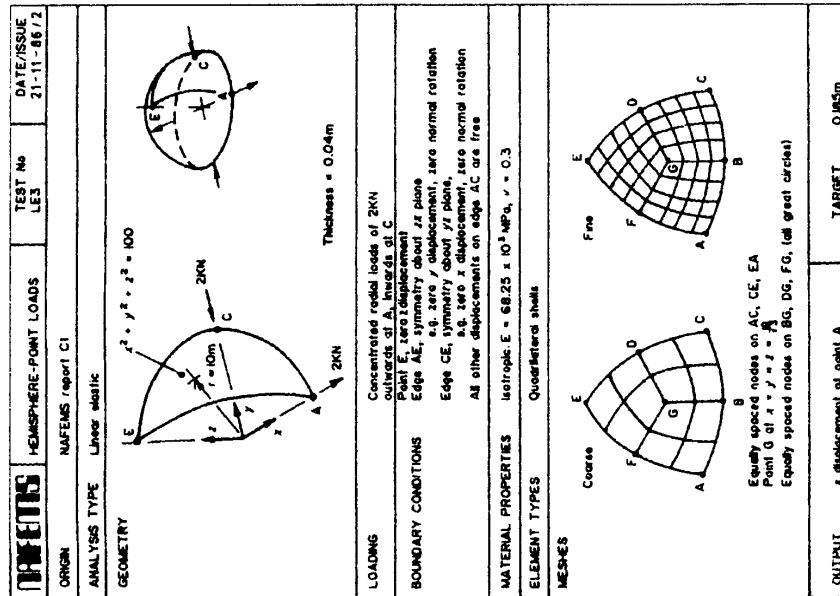


Figure 1. NAFEMS LE2

Element	Average Stress at E MPa	Percent Error	Standard Deviation	Standard Deviation Percent of Target
<b>Case 1, Bending</b>				
MB6	59.929	-0.118	0.489	0.185
AIZ6	52.752	-12.080	33.185	55.308
AIZ8	53.420	-10.968	6.204	10.340
MB4SI	58.126	-3.123	9.508	15.847
<b>Case 2, Membrane</b>				
MB6	59.931	-0.115	0.459	0.765
AIZ6	59.727	-0.455	0.702	1.170
AIZ8	56.278	-6.203	0.192	0.320
MB4SI	67.649	12.748	5.882	9.803

Table 1. NAFEMS LE2 Results





## NAFEMS LE3 [5] RESULTS

Target Deflection at A = 0.185m

Element	Coarse Mesh		Fine Mesh	
	Deflection m	Percent Error	Deflection m	Percent Error
MB6	0.18590	0.486	0.18451	-0.265
AIZ6	0.01484	-91.977	0.07540	-59.244
AIZ8	0.1385	-25.162	0.18458	-0.227
NASTR A def	0.215388	+16.43	0.213499	+15.40
NASTR A opt	0.188606	+1.95	0.185079	+0.04
NASTR B def	0.191657	+3.60	0.186641	+0.89
NASTR B opt	0.090387	-51.14	0.195662	+5.79
LU7IS	0.18801	1.630	-----	-----
MB4SI	0.06813	-63.174	0.17344	-6.249

Table 2. NAFEMS LE3 Results

Figure 2. NAFEMS LE3

## SCORDELIS-LO ROOF [1,2] RESULTS

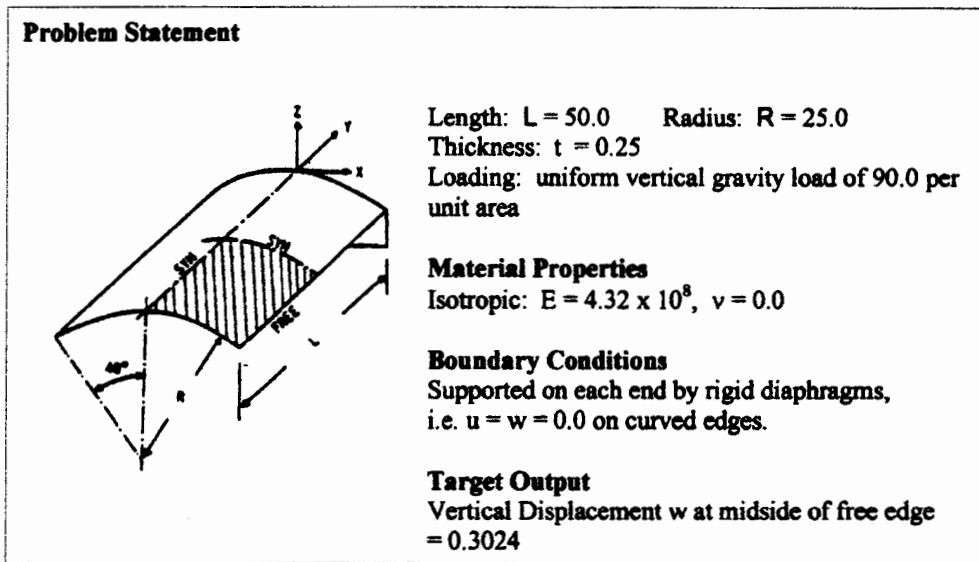


Figure 3(a) Scordelis-Lo Roof

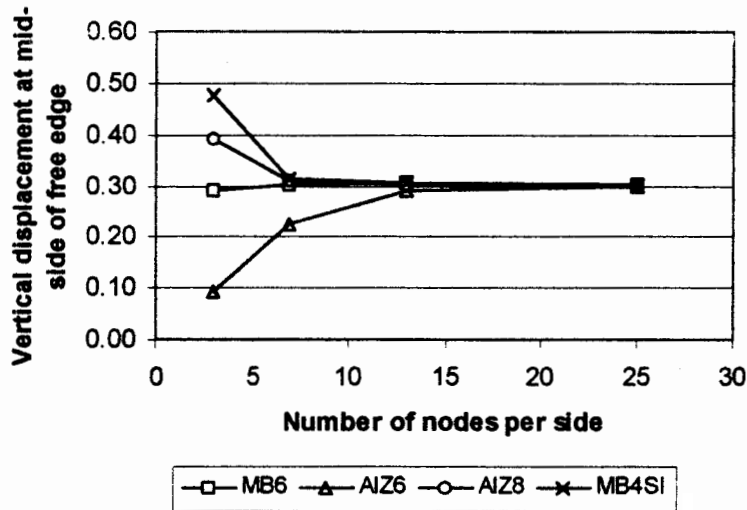
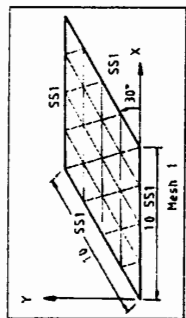


Figure 3(b) Scordelis-Lo Roof Results

Target Deflection = 0.3024 ft at mid-side of free edge

Nodes per Side	Vertical Deflection at Mid-Side of Free Edge (ft)			
	MB6	AIZ6	AIZ8	MB4SI
3	0.29178	0.09344	0.39091	0.47804
7	0.30244	0.22418	0.30960	0.31441
13	0.30495	0.28884	0.30364	0.30572
25	0.30377	0.29993	0.30232	0.30313

Table 3. Scordelis-Lo Roof Results



Objective: Compute the maximum deflection of a simply supported isotropic plate subject to a uniformly distributed load.

Figure 4(a) Morley Skew Plate

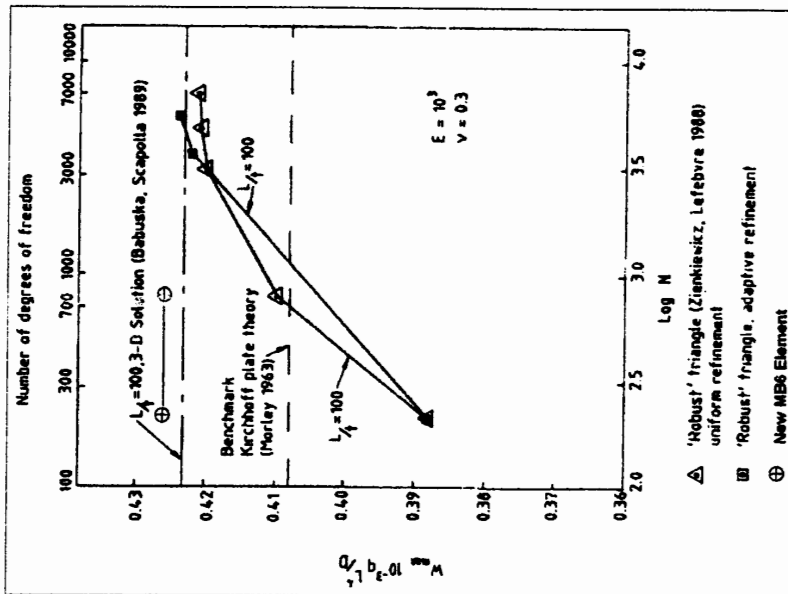


Figure 4(b) Morley Skew Plate Results

### MORLEY SKEW PLATE RESULTS [6]

Target: Babuska-Scapolla 3D  
 Normalized Deflection = 0.423

Source	DOF	Percent Error
Morley	NA	-3.6
MB6	211	0.8
REF [6]	211	-8.3
AIZ6	211	-18.4
AIZ8	211	-35.2
MB4SI	211	-4.0

Table 4. Morley Skew Plate Result

## PLUNKETT'S VIBRATING WEDGE [7] RESULTS

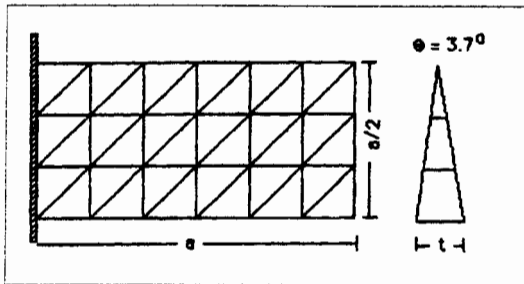


Figure 5. Plunkett's Vibrating Wedge

### Objective

Determine the first 12 out-of-plane modes of vibration for a cantilevered wedge section plate using a 3 x 6 mesh and consistent mass matrix.

### Material Properties

Isotropic:  $E = 10E6$ ,  $\nu = 0.3$ ,  $\rho = 0.0002591$

### Boundary Conditions

All degrees of freedom are fixed at support. All  $u, v$ , and  $\theta_z$  displacements are fixed to eliminate in-plane vibration modes.

### Geometry

$a = 30$ , thickness at tip = 0.001,  $t = 0.96899451$

### Results

Target: Experimental Data (normalized) for mode shapes similar to Plunkett's sketches.

Mode	Element	MB6	AIZ6	AIZ8	MB4SI
	Target Frequency	Percent Error			
1	2.47	-2.8	-2.4	-3.0	-3.1
2	10.6	4.4	6.9	2.1	-1.8
3	14.2	1.4	3.6	1.1	4.7
4	28.7	-0.9	7.7	-1.7	-5.6
5	34.4	-0.6	11.3	-1.0	-1.7
6	47.4	-4.7	13.9	-4.5	-9.5
7	52.5	-3.4	8.3	-9.1	
8	54.0	-1.9	18.1	-3.6	
9	63.5	-9.1	15.8		
10	68.0	-10.1	27.6		

Table5. Plunkett's Vibrating Wedge Results

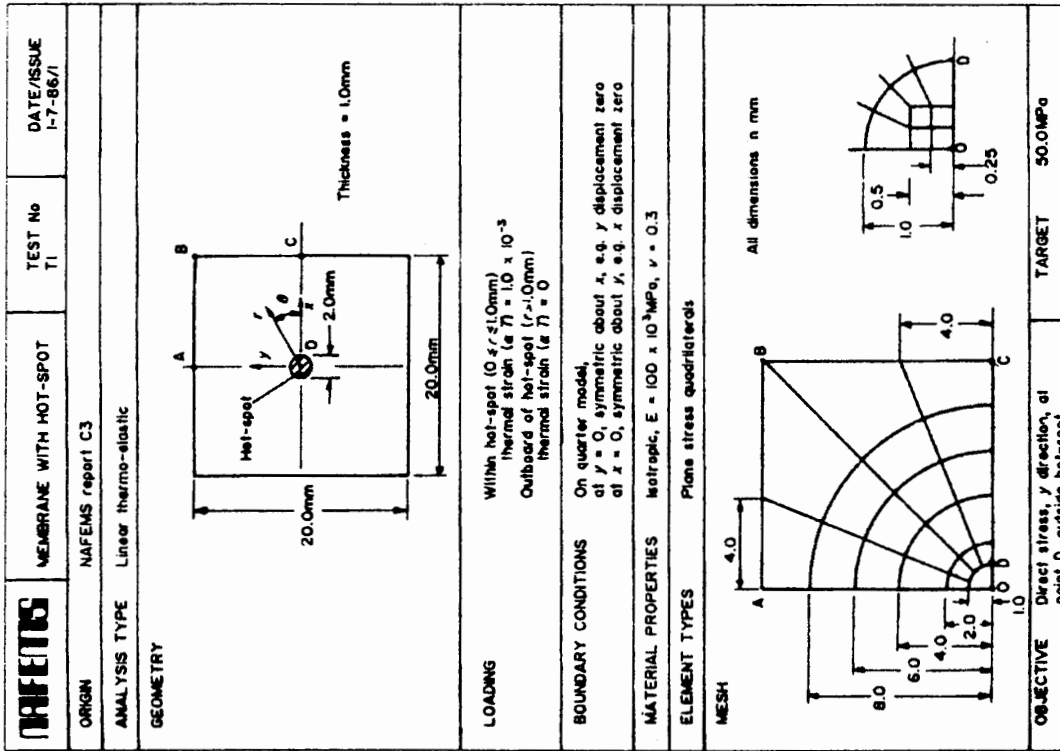


Figure 6, NAFEMS T1

## NAFEMS T1 [5] RESULTS

Target: Direct Stress,  $y$ -direction, at point D,  
outside hot spot = 50.0 MPa

Element	Stress at Node D (MPa)	
	FEA Solution	Percent Error
MB6	49.769	-0.46
AIZ6	49.911	-0.18
AIZ8	46.104	-7.79
MB4	70.909	41.82
MB4SI	50.661	1.32

Table 6. NAFEMS T1 Results

Version	Z Deflection At E (mm)	% Error	Bending Stress At E (MPa)	% Error	Interlaminar Shear Stress at D (MPa)	% Error
MB6	-1.0545	-0.5189	683.14	-0.1111	-4.00	-2.4390
MB10	-1.0544	-0.5283	684.60	0.1024	-4.01	-2.1951
AIZ6	-1.0541	-0.5566	684.74	0.1228	-4.07	-0.7317
AIZ8	-1.0544	-0.5283	684.23	0.0483	-4.10	0.0000
AIZ10	-1.0542	-0.5472	684.28	0.0556	-4.10	0.0000

Table 7 Results for NAFEMS Laminated Strip

NAFEMS	LAMINATED STRIP	Test No. 1	Date/ Issue draft
Origin	NAFEMS report		
Analysis type	Orthotropic		
Geometry	<p style="text-align: right;"><i>All dimensions in mm</i></p>		
Loading	Load line of 10N/mm at C (x=25, z=1)		
Boundary conditions	One quarter model, simply supported at A (z=0) and reflective symmetry about x=25 and about y=5		
Material properties	$E_1 = 1.0E5 \text{ MPa}$ , $\nu_{12} = 0.4$ , $E_2 = 5.0E3 \text{ MPa}$ , $\frac{\nu_{12}}{E_1} = \frac{\nu_{21}}{E_2}$ $G_{12} = 3.0E3 \text{ MPa}$ , $\nu_{23} = 0.3$ , $G_{33} = 2.0E3 \text{ MPa}$		
Element types	Laminated beam, laminated plate, laminated brick or stacked brick		
Meshes			
Output	Bending stress at E Interlaminar shear stress at D z deflection at E	Target	683.9 MPa -4.1 MPa -1.06 mm

Figure 7 NAFEMS Laminated strip

NAFEMS BENCHMARK TEST No. LE2					
For shells					
SYSTEM	CASE 1		CASE 2		
	Nodes		Nodes		
	4	8	4	8	
NASTRAN	-15.3	-10.5	-17.0	-6.0	
ANSYS	-18.0	+32.0	-55.0	+5.0	
GIFTS			+2.9		Membrane locking
MELINA	-98.2	-9.8	-2.3	-5.0	
MELISSA		-7.0		-6.2	
MARC	-4.2	-12.0	+10.8	-6.9	
PAFEC		+5.7		-1.6	
ASAS		-55.0		+4.5	
LUSAS	+4.0	+3.1	+7.6	+7.6	
FINEL		-10.0		+2.0	
SUPERTAB	-18.8	-25.8	-40.7	-15.8	
BERSAFE		-2.2		-8.2	Reduced integration
COSMOS/M	-6.3	-4.8*	-24.0	+3.3*	
ABAQUS	0.0	-0.3	+1.0	+0.8	
NISA	+2.6	-12.0	+11.0	-5.0	

Table 8a. NAFEMS LE2 Curved Shell Patch Test 1989 Results

NAFEMS BENCHMARK TEST No. LE3					
Hemisphere with pinch loading					
SYSTEM	COARSE		FINE		
	Nodes		Nodes		
	4	8	4	8	
NASTRAN	+3.2		+1.1	+3.2	
ANSYS		-19.4	0.0	+1.1	Warp flag
GIFTS	-49.6		-7.2		
MELINA		-5.4		-8.1	9-Node shell
MELISSA		-23.8		-0.5	
MARC	-65.9	-29.5	-11.8	-1.3	
PAFEC		-11.3		0.0	
ASAS					
LUSAS	-93.5	-9.7	-81.6	0.0	Full integration
FINEL		-3.1		-2.2	
SUPERTAB	+1.6	-31.9	-0.5	-4.3	
BERSAFE		-14.7		-0.1	Reduced integration
COSMOS	-11.3	+15.0*	-1.1	-1.6*	
ABAQUS	+3.2	-4.3	-1.1	0.0	
NISA	-9.5	-11.4	-17.3	+7.6	

Table 8b. NAFEMS LE3 Pinched Hemisphere Shell 1989 Results

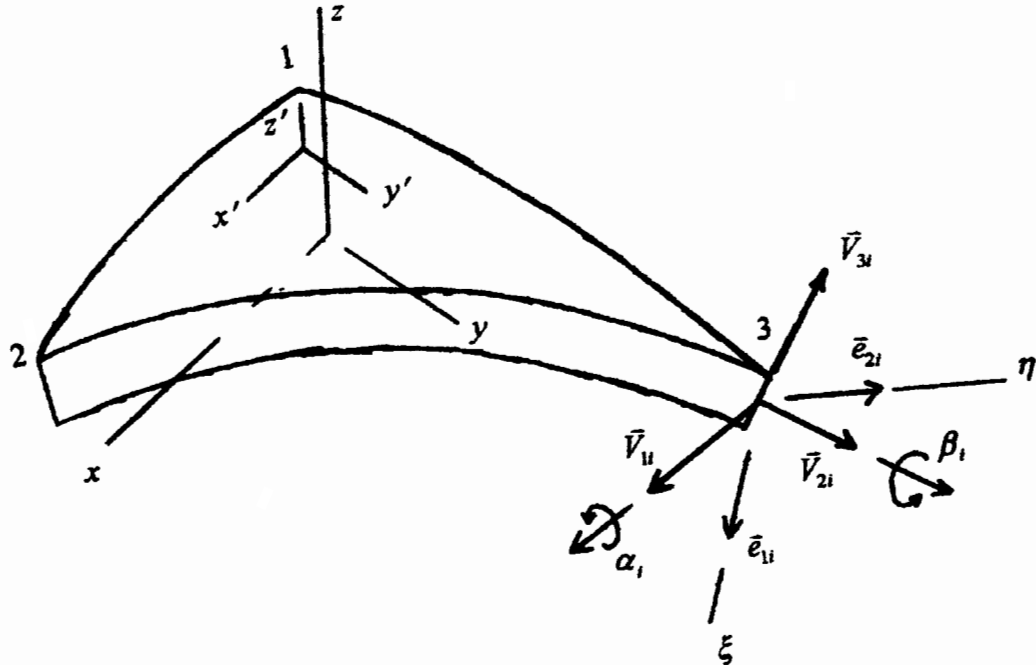
<b>ERROR SUMMARY TABLE – 6 AND 8 NODE ELEMENTS</b>									
<b>Percent Errors</b>									
	<b>MB6</b>	<b>AIZ6</b>	<b>AIZ8</b>	<b>NASTRAN “A” Default</b>	<b>NASTRAN “A” Option</b>	<b>NASTRAN “B” Default</b>	<b>NASTRAN “B” Option</b>	<b>NASTRAN “B” Default</b>	<b>NASTRAN “B” Option</b>
<b>NAFEMS LE2 Bending</b>	-0.12	-12.08	-10.97	-3.41		+1.88		+1.88	-7.85 (-12.68)
<b>NAFEMS LE2 Membrane</b>	-0.12	-0.46	-6.20	+85.33 (-99.3 to +100)		+15.32 (-53.3 to +15.32)		+15.32 (-53.3 to +15.32)	-2.03 (+82.0)
<b>NAFEMS LE3 Coarse</b>	+0.49	-91.98	-25.16	+16.43		+3.60	+1.95	+3.60	-51.14
<b>NAFEMS LE3 Fine</b>	-0.27	-59.24	-0.23	+15.40		+0.89	+0.04	+0.89	+5.76
<b>Scordelis-Lo Roof 7 Nodes per side</b>	+0.01	-25.87	+2.38	+0.90		-2.83		-2.83	+3.53
<b>Scordelis-Lo Roof 25 Nodes per side</b>	+0.45	-0.82	-0.03	-0.00		+9.55 DIVERGES		+9.55 DIVERGES	+0.66
<b>Morley Skew Plate 211 d. o. f.</b>	+0.80	-18.40	-35.20	+1.10					
<b>NAFEMS LE5</b>	+2.16	+1.89	+2.28			-17.75		-17.75	+3.72

**Table 9. Error Summary for 6 and 8 Node Elements on Six Critical Test Cases**



## Appendix A

### Curved Element Development



The element  $x$ - $y$  axis are in the plane defined by nodes 1-2-3, with origin at the centroid,  $x$  axis parallel to the 1-2 edge, and  $z$  axis perpendicular to the plane. The element matrices are developed in these axes.

Unit vectors,  $\bar{e}_1$  and  $\bar{e}_2$  tangent to the mid-surface at any point are

$$\begin{aligned} x_{,\xi} &= \sum N_{i,\xi} x_i \\ \bar{e}_1 = y_{,\xi} &= \sum N_{i,\xi} y_i \\ z_{,\xi} &= \sum N_{i,\xi} z_i \end{aligned}$$

[A1]

$$\begin{aligned} x_{,\eta} &= \sum N_{i,\eta} x_i \\ \bar{e}_2 = y_{,\eta} &= \sum N_{i,\eta} y_i \\ z_{,\eta} &= \sum N_{i,\eta} z_i \end{aligned}$$

Where  $x_i, y_i, z_i$  are coordinates of nodes and  $N_i$  are conventional interpolation functions.

$$\bar{V}_2 = \frac{\bar{V}_3 \times \bar{i}}{|\bar{V}_3 \times \bar{i}|} = \begin{bmatrix} l_2 \\ m_2 \\ n_2 \end{bmatrix}$$

$$\bar{V}_3 = \frac{\bar{e}_1 \times \bar{e}_2}{|\bar{e}_1 \times \bar{e}_2|} = \begin{bmatrix} l_3 \\ m_3 \\ n_3 \end{bmatrix}$$

[A2]

$$\bar{V}_1 = \bar{V}_2 \times \bar{V}_3 = \begin{bmatrix} l_1 \\ m_1 \\ n_1 \end{bmatrix}$$

The local axis  $x'-y'-z'$  at any point are the directions of  $\bar{V}_1$ ,  $\bar{V}_2$ , and  $\bar{V}_3$ , respectively.

Rotations in element axis are

$$\begin{bmatrix} \theta_x \\ \theta_y \\ \theta_z \end{bmatrix} = \begin{bmatrix} l_1 & l_2 & l_3 \\ m_1 & m_2 & m_3 \\ n_1 & n_2 & n_3 \end{bmatrix} \begin{bmatrix} \alpha \\ \beta \\ 0 \end{bmatrix}$$

[A3]

In a flat element

$$\bar{V}_1 = \bar{i}, \quad \bar{V}_2 = \bar{j}, \quad \alpha = \theta_x \quad \text{and} \quad \beta = \theta_y.$$

With these definitions, the material property transformations can be done as in a flat element, provided that, the angle  $\phi$  which is input is the angle between the local  $x'$  axis and the fiber direction.

### ***Curved Element Development***

$$\begin{aligned}
 x &= \sum_{i=1}^n N_i x_i + \sum_{i=1}^n N_i \zeta \frac{1}{2} t_i l_{3i} \\
 y &= \sum_{i=1}^n N_i y_i + \sum_{i=1}^n N_i \zeta \frac{1}{2} t_i m_{3i} \\
 z &= \sum_{i=1}^n N_i z_i + \sum_{i=1}^n N_i \zeta \frac{1}{2} t_i n_{3i}
 \end{aligned} \tag{A4}$$

Where  $n$  is the number of nodes in an element.

Displacements in the element  $x$ - $y$ - $z$  axis are

$$\begin{aligned}
 u &= \sum_{i=1}^n N_i u_i + \frac{1}{2} t \zeta \sum_{i=1}^n N_i [-l_{2i} \alpha_i + l_{1i} \beta_i] \\
 v &= \sum_{i=1}^n N_i v_i + \frac{1}{2} t \zeta \sum_{i=1}^n N_i [-m_{2i} \alpha_i + m_{1i} \beta_i] \\
 w &= \sum_{i=1}^n N_i w_i + \frac{1}{2} t \zeta \sum_{i=1}^n N_i [-n_{2i} \alpha_i + n_{1i} \beta_i]
 \end{aligned} \tag{A5}$$

Where

$$\sum_{i=1}^n N_i [-l_{2i} \alpha + l_{1i} \beta] \quad , \quad \sum_{i=1}^n N_i [-m_{2i} \alpha + m_{1i} \beta] \quad , \quad \sum_{i=1}^n N_i [-n_{2i} \alpha + n_{1i} \beta]$$

interpolates rotations of normal lines. This differs from Ahmad-Irons-Zienkiewicz in that interpolated nodal rotations are multiplied by the local thickness,  $t$ , scaled by  $\zeta$  to produce a contribution to  $u$ ,  $v$ , and  $w$ . This is significant only in variable thickness elements. Note that both rotations and displacements are defined at the middle surface, and the Jacobian  $J$  should be evaluated there.

The transformation of rotations from the local axis  $\alpha_i$ , and  $\beta_i$ , to the element axis  $\theta_x$ ,  $\theta_y$ ,  $\theta_z$  is

$$\begin{bmatrix} \alpha_i \\ \beta_i \\ 0 \end{bmatrix} = \begin{bmatrix} l_{1i} & m_{1i} & n_{1i} \\ l_{2i} & m_{2i} & n_{2i} \\ l_{3i} & m_{3i} & n_{3i} \end{bmatrix} \begin{bmatrix} \bar{\theta}_{xi} \\ \bar{\theta}_{yi} \\ \bar{\theta}_{zi} \end{bmatrix} = \mathbf{T}_i \bar{\boldsymbol{\theta}}_i \quad [\text{A6}]$$

The Jacobian  $\mathbf{J}$  is

$$\mathbf{J} = \begin{bmatrix} x_{,\xi} & y_{,\xi} & z_{,\xi} \\ x_{,\eta} & y_{,\eta} & z_{,\eta} \\ x_{,\zeta} & y_{,\zeta} & z_{,\zeta} \end{bmatrix} \quad [\text{A7}]$$

Where

$$x_{,\xi} = \sum_{i=1}^n N_{i,\xi} x_i + \sum_{i=1}^n N_{i,\xi} \frac{1}{2} \zeta_i l_{3i}$$

$$x_{,\eta} = \sum_{i=1}^n N_{i,\eta} x_i + \sum_{i=1}^n N_{i,\eta} \frac{1}{2} \zeta_i l_{3i} \quad [\text{A8}]$$

$$x_{,\zeta} = \sum_{i=1}^n N_i \frac{1}{2} \zeta_i l_{3i}$$

Etc. where  $n$  = number of nodes.

In the new element versions stiffness matrix, the Jacobian  $\mathbf{J}$  is always evaluated at the mid-surface,  $\zeta = 0$ , so the terms containing  $\zeta$  after differentiation vanish.

Let (for 4-node case) (other cases similar)

$$\mathbf{R}_u = \begin{bmatrix} -l_{21} & l_{11} & 0 & 0 & 0 & 0 & 0 & 0 & 0 & 0 & 0 & 0 \\ 0 & 0 & 0 & -l_{22} & l_{12} & 0 & 0 & 0 & 0 & 0 & 0 & 0 \\ 0 & 0 & 0 & 0 & 0 & 0 & -l_{23} & l_{13} & 0 & 0 & 0 & 0 \\ 0 & 0 & 0 & 0 & 0 & 0 & 0 & 0 & 0 & -l_{24} & l_{14} & 0 \end{bmatrix} \begin{bmatrix} \mathbf{T}_1 & 0 & 0 & 0 \\ 0 & \mathbf{T}_2 & 0 & 0 \\ 0 & 0 & \mathbf{T}_3 & 0 \\ 0 & 0 & 0 & \mathbf{T}_4 \end{bmatrix} \quad [\text{A9}]$$

$$\mathbf{R}_w = \begin{bmatrix} -n_{21} & n_{11} & 0 & 0 & 0 & 0 & 0 & 0 & 0 & 0 & 0 & 0 \\ 0 & 0 & 0 & -n_{22} & n_{12} & 0 & 0 & 0 & 0 & 0 & 0 & 0 \\ 0 & 0 & 0 & 0 & 0 & 0 & -n_{23} & n_{13} & 0 & 0 & 0 & 0 \\ 0 & 0 & 0 & 0 & 0 & 0 & 0 & 0 & 0 & -n_{24} & n_{14} & 0 \end{bmatrix} \begin{bmatrix} \mathbf{T}_1 & 0 & 0 & 0 \\ 0 & \mathbf{T}_2 & 0 & 0 \\ 0 & 0 & \mathbf{T}_3 & 0 \\ 0 & 0 & 0 & \mathbf{T}_4 \end{bmatrix}$$

$$\mathbf{R}_v = \begin{bmatrix} -m_{21} & m_{11} & 0 & 0 & 0 & 0 & 0 & 0 & 0 & 0 & 0 & 0 \\ 0 & 0 & 0 & -m_{22} & m_{12} & 0 & 0 & 0 & 0 & 0 & 0 & 0 \\ 0 & 0 & 0 & 0 & 0 & 0 & -m_{23} & m_{13} & 0 & 0 & 0 & 0 \\ 0 & 0 & 0 & 0 & 0 & 0 & 0 & 0 & -m_{24} & m_{14} & 0 & 0 \end{bmatrix} \begin{bmatrix} T_1 & 0 & 0 & 0 \\ 0 & T_2 & 0 & 0 \\ 0 & 0 & T_3 & 0 \\ 0 & 0 & 0 & T_4 \end{bmatrix}$$

Therefore, the displacements within our element can be expressed as a function of the nodal displacements by

$$\begin{bmatrix} u \\ v \\ w \end{bmatrix} = \begin{bmatrix} N & 0 & 0 & \frac{1}{2}\zeta t N R_u \\ 0 & N & 0 & \frac{1}{2}\zeta t N R_v \\ 0 & 0 & N & \frac{1}{2}\zeta t N R_w \end{bmatrix} \begin{bmatrix} \bar{u} \\ \bar{v} \\ \bar{w} \\ \bar{\theta} \end{bmatrix} \quad [\text{A10}]$$

Where, for the 4-node case,

$$\bar{\mathbf{u}}^T = [\bar{u}_1 \quad \bar{u}_2 \quad \bar{u}_3 \quad \bar{u}_4]$$

$$\bar{\mathbf{v}}^T = [\bar{v}_1 \quad \bar{v}_2 \quad \bar{v}_3 \quad \bar{v}_4]$$

[A11]

$$\bar{\mathbf{w}}^T = [\bar{w}_1 \quad \bar{w}_2 \quad \bar{w}_3 \quad \bar{w}_4]$$

$$\bar{\boldsymbol{\theta}}^T = [\bar{\theta}_{x1} \quad \bar{\theta}_{y1} \quad \bar{\theta}_{z1} \quad \bar{\theta}_{x2} \quad \bar{\theta}_{y2} \quad \bar{\theta}_{z2} \quad \bar{\theta}_{x3} \quad \bar{\theta}_{y3} \quad \bar{\theta}_{z3} \quad \bar{\theta}_{x4} \quad \bar{\theta}_{y4} \quad \bar{\theta}_{z4}]$$

To get the strains we differentiate  $u$ ,  $v$ , and  $w$ , for example

$$u_{, \xi} = \begin{bmatrix} N_{, \xi} & 0 & 0 & \frac{1}{2}\zeta t N_{, \xi} R_u \end{bmatrix} \begin{bmatrix} \bar{u} \\ \bar{v} \\ \bar{w} \\ \bar{\theta} \end{bmatrix} + \begin{bmatrix} 0 & 0 & 0 & \frac{1}{2}\zeta t_{, \xi} N R_u \end{bmatrix} \begin{bmatrix} \bar{u} \\ \bar{v} \\ \bar{w} \\ \bar{\theta} \end{bmatrix} \quad [\text{A12}]$$

Terms involving the derivatives of  $t$  such as the  $t_{, \xi}$  have been neglected since they give strains due to rigid body motion. These derivatives vanish when the element thickness is constant. This formulation is used to avoid singularity due to very thin edges. The Ahmad-Irons-Zienkiewicz formulation may be a bit better for thick elements.

The derivatives of the displacement functions may be computed at any point as

$$\begin{bmatrix} u_{,\xi} \\ u_{,\eta} \\ u_{,\zeta} \\ v_{,\xi} \\ v_{,\eta} \\ v_{,\zeta} \\ w_{,\xi} \\ w_{,\eta} \\ w_{,\zeta} \end{bmatrix} = \begin{bmatrix} N_{,\xi} & 0 & 0 & \frac{1}{2}\zeta t N_{,\xi} R_u \\ N_{,\eta} & 0 & 0 & \frac{1}{2}\zeta t N_{,\eta} R_u \\ 0 & 0 & 0 & \frac{1}{2}t N R_u \\ 0 & N_{,\xi} & 0 & \frac{1}{2}\zeta t N_{,\xi} R_v \\ 0 & N_{,\eta} & 0 & \frac{1}{2}\zeta t N_{,\eta} R_v \\ 0 & 0 & 0 & \frac{1}{2}t N R_v \\ 0 & 0 & N_{,\xi} & \frac{1}{2}\zeta t N_{,\xi} R_w \\ 0 & 0 & N_{,\eta} & \frac{1}{2}\zeta t N_{,\eta} R_w \\ 0 & 0 & 0 & \frac{1}{2}t N R_w \end{bmatrix} \begin{bmatrix} \bar{u} \\ \bar{v} \\ \bar{w} \\ \bar{\theta} \end{bmatrix} \quad [\text{A13}]$$

Note that this matrix can be divided into a part including  $\zeta$  and a part not including  $\zeta$

$$\begin{bmatrix} \varepsilon'_x \\ \varepsilon'_y \\ \varepsilon'_z \\ \varepsilon'_{xy} \\ \varepsilon'_{yz} \\ \varepsilon'_{zx} \end{bmatrix} = T_\varepsilon H \begin{bmatrix} J^{-1} & 0 & 0 \\ 0 & J^{-1} & 0 \\ 0 & 0 & J^{-1} \end{bmatrix} \begin{bmatrix} u_{,\xi} \\ u_{,\eta} \\ u_{,\zeta} \\ v_{,\xi} \\ v_{,\eta} \\ v_{,\zeta} \\ w_{,\xi} \\ w_{,\eta} \\ w_{,\zeta} \end{bmatrix} \quad [\text{A14}]$$

Matrix  $H$  above transforms derivatives to strains in the element ( $x$ - $y$ - $z$ ) axis (Cook, p. 360) and matrix  $T_\varepsilon$  transforms strains to local ( $x'$ - $y'$ - $z'$ ) axis (Cook, p. 212).

Combining these equations, we can write

$$\varepsilon' = [B_0 + \zeta B_1] \begin{bmatrix} \bar{u} \\ \bar{v} \\ \bar{w} \\ \bar{\theta} \end{bmatrix} \quad [\text{A15}]$$

Where strains are in the local  $x'-y'-z'$  axis.

The stiffness matrix (integrated in local axis) is then

$$\mathbf{K} = \int_V \mathbf{B}^T \mathbf{D}' \mathbf{B} [\text{Det } \mathbf{J}] d\xi d\eta d\zeta \quad [\text{A16}]$$

Only the stretching and bending parts of the stiffness matrix are computed from this expression in our elements. The out-of-plane shearing stiffness is computed from a different process.

In these equations, the Jacobian,  $\mathbf{J}$ , is evaluated at the middle surface.

Note that explicit integration through the thickness is possible.

$$\begin{aligned} \mathbf{K} &= \int [\mathbf{B}'_o + \zeta t \mathbf{B}'_1] \mathbf{D}' [\mathbf{B}'_o + \zeta t \mathbf{B}'_1] [\text{Det } \mathbf{J}] d\xi d\eta d\zeta \\ &= \int \mathbf{B}'_o \mathbf{D}' \mathbf{B}'_o [\text{Det } \mathbf{J}] d\xi d\eta d\zeta + \int \mathbf{B}'_1 [\zeta^2 t^2 \mathbf{D}'] \mathbf{B}'_1 [\text{Det } \mathbf{J}] d\xi d\eta d\zeta \\ &\quad + \int [\mathbf{B}'_o [\zeta t \mathbf{D}'] \mathbf{B}'_1 + \mathbf{B}'_1 [\zeta t \mathbf{D}'] \mathbf{B}'_o] [\text{Det } \mathbf{J}] d\xi d\eta d\zeta \end{aligned} \quad [\text{A17}]$$

$\mathbf{B}'_o$  contains  $t$ , but in the form above,  $t$  is factored out of  $\mathbf{B}'_1$ .

$$\begin{aligned} \int_{-1}^1 \mathbf{D}' d\zeta &= \sum_{j=1}^{NLAY} \mathbf{D}'_j (\zeta_j - \zeta_{j-1}) \\ \int_{-1}^1 \mathbf{D}' \zeta d\zeta &= \int_{-1}^{\zeta_1} \mathbf{D}'_1 \zeta d\zeta + \int_{\zeta_1}^{\zeta_2} \mathbf{D}'_2 \zeta d\zeta + \dots \\ &= \mathbf{D}'_1 \left[ \frac{\zeta^2}{2} \right]_{-1}^{\zeta_1} + \mathbf{D}'_2 \left[ \frac{\zeta^2}{2} \right]_{\zeta_1}^{\zeta_2} + \dots \\ &= \sum_{j=1}^{NLAY} \frac{1}{2} \mathbf{D}'_j (\zeta_j^2 - \zeta_{j-1}^2) \end{aligned} \quad [\text{A18}]$$

$$\int_{-1}^1 \mathbf{D}' \zeta^2 d\zeta = \sum_{j=1}^{NLAY} \frac{1}{3} \mathbf{D}'_j (\zeta_j^3 - \zeta_{j-1}^3)$$

In a sandwich structure with constant-thickness skins and variable-thickness core, the integrals

$$\int_{-1}^1 \mathbf{D}' d\zeta, \quad \int_{-1}^1 \mathbf{D}' \zeta d\zeta, \quad \text{and} \quad \int_{-1}^1 \mathbf{D}' \zeta^2 d\zeta$$

would have different values at each integration point.

To complete the integration of

$$\begin{aligned}
 \mathbf{K} = & \int \mathbf{B}_o^T \left[ \int_{-1}^1 \mathbf{D}' d\zeta \right] \mathbf{B}_o \text{Det}[\mathbf{J}] d\xi d\eta \\
 & + \int \mathbf{B}_1^T t^2 \left[ \int_{-1}^1 \mathbf{D}' \zeta^2 d\zeta \right] \mathbf{B}_1 \text{Det}[\mathbf{J}] d\xi d\eta \\
 & + \int \left[ \mathbf{B}_o^T t \left[ \int_{-1}^1 \mathbf{D}' \zeta d\zeta \right] \mathbf{B}_1 + \mathbf{B}_1^T t \left[ \int_{-1}^1 \mathbf{D}' \zeta d\zeta \right] \mathbf{B}_o \right] \text{Det}[\mathbf{J}] d\xi d\eta
 \end{aligned} \tag{A19}$$

does not require multiple points in the through-thickness direction. The computing time could be considerably reduced, compared to using two points per layer in the through-thickness direction.



## Appendix B

### Modifications to $B_o$

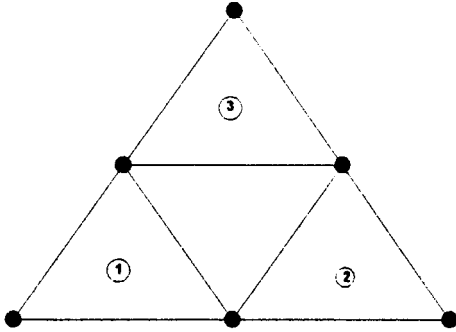
In curved quadratic elements, bending causes spurious mid-surface strains, except at the  $2 \times 2$  Gauss points. These spurious strains cause serious errors in fully integrated Ahmad-Irons-Zienkiewicz elements when the “rise” (deviation from flatness) of the element is more than about 1/5 of its thickness.

It has been observed that, in constant-curvature bending of quadratic elements, the average mid-surface strains is (correctly) zero. Thus, the spurious mid-surface strain which causes excessive bending stiffness can be avoided by replacing  $B_o$  with

$$B_{oAVG} = \sum_{k=1}^m W_k B_{ok} \quad [B1]$$

where  $m$  is the number of integration points over  $\xi$  and  $\eta$  and  $W_k$  are the integration weights.

Unfortunately, this eliminates the gradient in mid-surface strains which is needed for accurate solution to some problems. It also introduces mechanisms.



In the 6-node triangular element, the gradient can be restored by using triangular subregions. Using 3-point integration for the 6-node triangle, the integration points coincide with centroids of the 3 corner subregions. Denoting the strain-displacement matrices of the three subregions by  $B_1^*$ ,  $B_2^*$ ,  $B_3^*$ , the membrane strain gradient is restored by using:

$$B_{ok} = B_{oAVG} + B_k^* - \sum_{k=1}^3 \frac{1}{3} B_k^* \quad [B2]$$

It can be shown that this gives exactly correct membrane strains for all constant strain states and all linear strain states in a

flat 6-node triangle with straight sides. No mechanisms are introduced by this process. Strain-displacement matrices are computed for the 3 corner subregions as flat 3-dimensional constant strain triangles.

## Appendix C

### *Shear Perpendicular to Surface in Flat Elements*

In Mindlin plate theory, shear perpendicular to the surface is given by

$$\begin{aligned}\gamma_{yz} &= \frac{\partial w}{\partial y} - \Theta_x \\ \gamma_{xz} &= \frac{\partial w}{\partial x} + \Theta_y\end{aligned}\tag{C.1}$$

Sign conventions for displacements and shear strains are shown in Figure C.1.

It is evident from equations C.1 that the function representing  $w$  should be one order higher than the functions representing  $\Theta_x$  and  $\Theta_y$ . Some conventional element nodal configurations and the terms appearing in interpolation functions are shown in Figure C.2. The solid lines bound terms in the conventional interpolation functions used for  $\Theta_x$  and  $\Theta_y$ , and the dashed lines bound terms required in the “unconventional” interpolation functions used for  $w$  by Family 1 elements.

All elements considered here have three degrees of freedom at each node: displacement  $w$ , rotation  $\Theta_x$ , and rotation  $\Theta_y$ . Rotations are always represented by conventional interpolation functions which are continuous on and across element boundaries. Bending strain energy is computed from rotation interpolation functions in the conventional manner.

#### *Element Family 1*

Following Utku (1) we choose

$$w = w' + w^*\tag{C.2}$$

in which  $w'$  represents bending or “Kirchhoffian” deflection and  $w^*$  represents shearing deflection.

$$\begin{aligned}\frac{\partial w}{\partial x} &= \frac{\partial w'}{\partial x} + \frac{\partial w^*}{\partial x} \\ \frac{\partial w}{\partial y} &= \frac{\partial w'}{\partial y} + \frac{\partial w^*}{\partial y}\end{aligned}\tag{C.3}$$

When shear deformation is zero we see from Figure C.1 that

$$\begin{aligned}\frac{\partial w}{\partial x} &= -\Theta_y = \frac{\partial w'}{\partial x} \\ \frac{\partial w}{\partial y} &= \Theta_x = \frac{\partial w'}{\partial y}\end{aligned}\tag{C.3a}$$

Using C.3

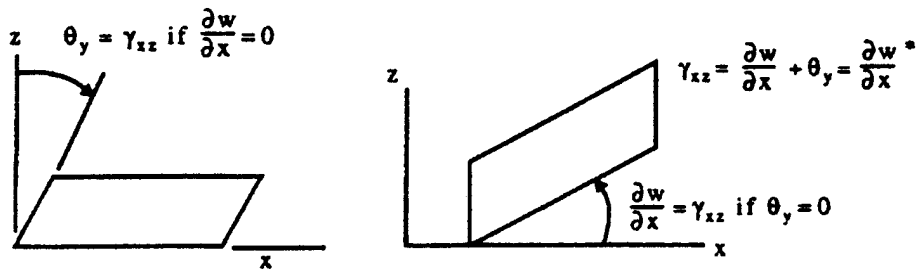
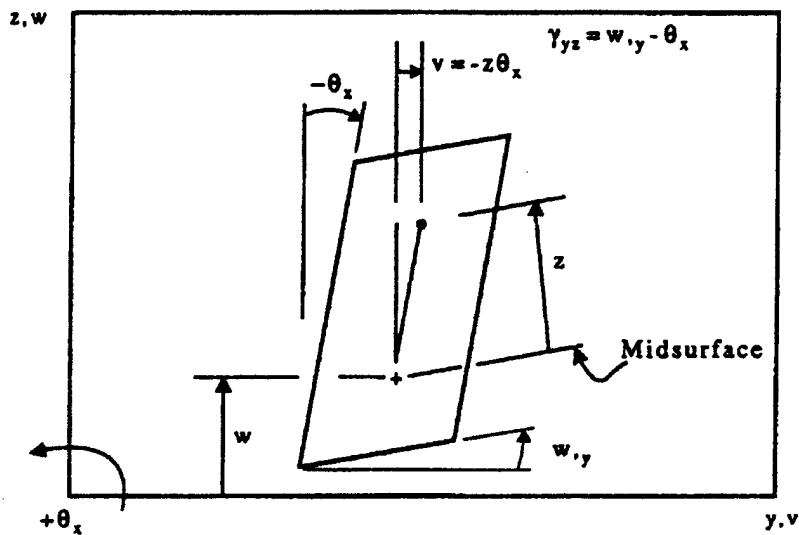
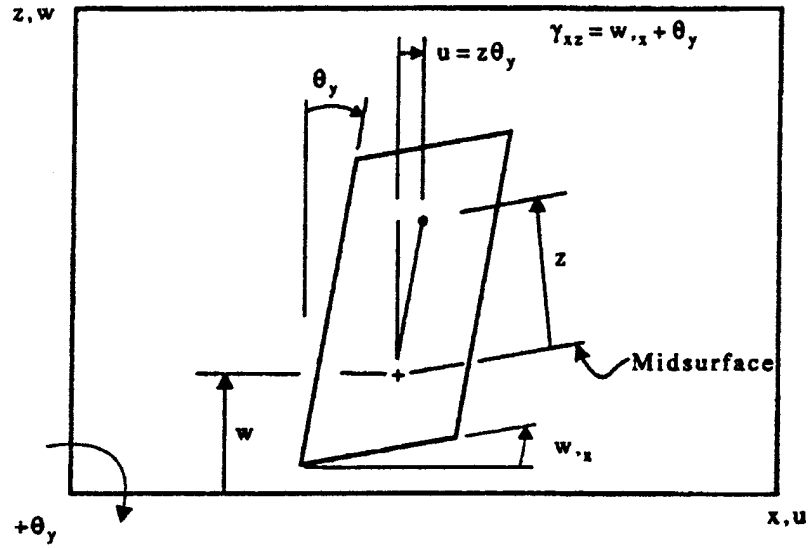


Figure C.1 Sign Conventions and Shear Deformation Relations


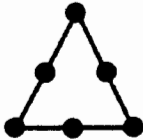
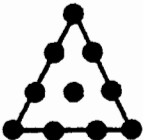
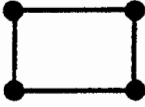
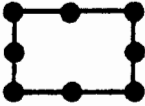
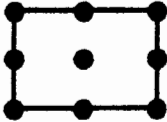
Nodal Configuration	Terms Included in Interpolation	Number Equations Available	Number Unknowns Family 1
	$\frac{1}{x^2 \frac{xy}{x'y} y^2}$	6	5
	$\frac{1}{x^2 \frac{xy}{x'y} y^2}$	12	9
	$\frac{1}{x^2 \frac{xy}{x'y} y^2}$	20	14
	$\frac{1}{x^2 \frac{xy}{x'y} y^2}$	8	7
	$\frac{1}{x^2 \frac{xy}{x'y} y^2}$	16	12
	$\frac{1}{x^2 \frac{xy}{x'y} y^2}$	18	14

Figure C.2 Nodal Configurations and Interpolation Terms

$$\begin{aligned}\frac{\partial w^*}{\partial x} &= \frac{\partial w}{\partial x} + \Theta_y = \gamma_{xz} \\ \frac{\partial w^*}{\partial y} &= \frac{\partial w}{\partial y} - \Theta_x = \gamma_{yz}\end{aligned}\tag{C.3.b}$$

In Figure C.1 it is shown that

$$\begin{aligned}\gamma_{xz} &= \Theta_y, \text{ when } \frac{\partial w}{\partial x} = 0 \\ \gamma_{yz} &= \frac{\partial w}{\partial y}, \text{ when } \Theta_x = 0\end{aligned}$$

so the choice of functions in Eq. C.2 is acceptable.

The method of Element Family 1 will be illustrated by application to the four-node element.

The conventional, continuous functions used for  $\Theta$  are

$$\begin{aligned}\Theta_x &= a_0 + a_1x + a_2y + a_3xy \\ \Theta_y &= b_0 + b_1x + b_2y + b_3xy\end{aligned}\tag{C.4}$$

The function for  $w'$  is chosen to contain terms one order higher:

$$w' = c_0 + c_1x + c_2y + c_3xy + c_4x^2 + c_5y^2 + c_6x^2y + c_7y^2x\tag{C.5}$$

An immediate problem arises, since differentiation of  $w'$  does not yield exactly the desired expressions for  $\Theta_x$  and  $\Theta_y$ ,

$$\Theta_x = \frac{\partial w'}{\partial y} = c_2 + c_3x + 2c_5y + c_6x^2 + 2c_7yx\tag{C.6}$$

The coefficients can be identified with those in Eq. C.4 except for term  $c_6x^2$ .

$$-\Theta_y = \frac{\partial w'}{\partial x} = c_1 + c_3y + 2c_4x + 2c_6xy + c_7y^2\tag{C.7}$$

Again, coefficients can be identified with those in Eq. C.4, except for term  $c_7y^2$ .

Another conflict which arises is that  $c_3$  corresponds to both  $a_1$  and  $b_2$  in Eq. C.4. Utku resolved this problem in his three-node element by using an average value.

Numerous attempts have failed to find a way to eliminate these conflicts. However, it appears that they do not prevent reaching the goal of representing all constant strain states exactly.

For pure bending in the  $y$ - $z$  plane

$$\frac{\partial^2 w'}{\partial y^2} = 2c_5 + 2c_7x = \text{constant}\tag{C.8a}$$

which requires that  $c_7 = 0$  for this pure bending state. For pure bending in the  $x$ - $z$  plane

$$\frac{\partial^2 w'}{\partial x^2} = 2c_4 + 2c_6y = \text{constant}\tag{C.8b}$$

which requires that  $c_6 = 0$  for this pure bending state.

For pure twist

$$\frac{\partial^2 w'}{\partial x \partial y} = c_3 + 2c_6x + 2c_7y \quad (C.9)$$

which requires that  $c_6$  and  $c_7 = 0$ .

To compute the values of the  $c_i$ , we require that Eq. C.6 and Eq. C.7 be satisfied at the nodal points. The bar above a symbol designates nodal values of the variable.

$$\begin{bmatrix} \bar{\Theta}_{x1} \\ \bar{\Theta}_{x2} \\ \bar{\Theta}_{x3} \\ \bar{\Theta}_{x4} \\ \bar{\Theta}_{y1} \\ \bar{\Theta}_{y2} \\ \bar{\Theta}_{y3} \\ \bar{\Theta}_{y4} \end{bmatrix} = \begin{bmatrix} 0 & 1 & x_1 & 0 & 2y_1 & x_1^2 & 2y_1x_1 \\ 0 & 1 & x_2 & 0 & 2y_2 & x_2^2 & 2y_2x_2 \\ 0 & 1 & x_3 & 0 & 2y_3 & x_3^2 & 2y_3x_3 \\ 0 & 1 & x_4 & 0 & 2y_4 & x_4^2 & 2y_4x_4 \\ -1 & 0 & -y_1 & -2x_1 & 0 & -2x_1y_1 & -y_1^2 \\ -1 & 0 & -y_2 & -2x_2 & 0 & -2x_2y_2 & -y_2^2 \\ -1 & 0 & -y_3 & -2x_3 & 0 & -2x_3y_3 & -y_3^2 \\ -1 & 0 & -y_4 & -2x_4 & 0 & -2x_4y_4 & -y_4^2 \end{bmatrix} \begin{bmatrix} c_1 \\ c_2 \\ c_3 \\ c_4 \\ c_5 \\ c_6 \\ c_7 \end{bmatrix} \quad (C.10)$$

Denoting the  $8 \times 7$  matrix above as  $\mathbf{A}$

$$\bar{\Theta} = \mathbf{A} \mathbf{c}$$

$$\mathbf{A}^T \bar{\Theta} = \mathbf{A}^T \mathbf{A} \mathbf{c}$$

$$\mathbf{c} = [\mathbf{A}^T \mathbf{A}]^{-1} \mathbf{A}^T \bar{\Theta} \quad (C.11)$$

This is a least-squares solution for  $\mathbf{c}$ .

$$w' = c_0 + [x \ y \ xy \ x^2 \ y^2 \ x^2y \ xy^2] [\mathbf{A}^T \mathbf{A}]^{-1} \mathbf{A}^T \bar{\Theta} \quad (C.12)$$

Note that additional terms could be added to  $w'$ , and Eq. C.10 can be solved if Matrix  $\mathbf{A}$  has at least as many rows as it has columns.

Interpolating  $w^*$  by the same function as  $\Theta_x$  and  $\Theta_y$

$$w^* = d_0 + d_1x + d_2y + d_3xy$$

$$w = w^* + w' \quad (C.13)$$

Combining  $c_0$  with  $d_0$

$$w = [1 \ x \ y \ xy] \mathbf{d} + [x \ y \ xy \ x^2 \ y^2 \ x^2y \ xy^2] [\mathbf{A}^T \mathbf{A}]^{-1} \mathbf{A}^T \bar{\Theta} \quad (C.14)$$

$$\begin{bmatrix} \bar{w}_1 \\ \bar{w}_2 \\ \bar{w}_3 \\ \bar{w}_4 \end{bmatrix} = \begin{bmatrix} 1 & x_1 & y_1 & x_1 y_1 \\ 1 & x_2 & y_2 & x_2 y_2 \\ 1 & x_3 & y_3 & x_3 y_3 \\ 1 & x_4 & y_4 & x_4 y_4 \end{bmatrix} \begin{bmatrix} d_0 \\ d_1 \\ d_2 \\ d_3 \end{bmatrix} + \begin{bmatrix} x_1 & y_1 & x_1 y_1 & x_1^2 & y_1^2 & x_1^2 y_1 & x_1 y_1^2 \\ x_2 & y_2 & x_2 y_2 & x_2^2 & y_2^2 & x_2^2 y_2 & x_2 y_2^2 \\ x_3 & y_3 & x_3 y_3 & x_3^2 & y_3^2 & x_3^2 y_3 & x_3 y_3^2 \\ x_4 & y_4 & x_4 y_4 & x_4^2 & y_4^2 & x_4^2 y_4 & x_4 y_4^2 \end{bmatrix} [\mathbf{A}^T \mathbf{A}]^{-1} \mathbf{A}^T \bar{\Theta} \quad (\text{C.15})$$

or

$$\begin{aligned}
\bar{\mathbf{w}} &= \mathbf{B} \mathbf{d} + \mathbf{C} [\mathbf{A}^T \mathbf{A}]^{-1} \mathbf{A}^T \bar{\Theta} \\
\mathbf{B}^T \bar{\mathbf{w}} &= \mathbf{B}^T \mathbf{B} \mathbf{d} + \mathbf{B}^T \mathbf{C} [\mathbf{A}^T \mathbf{A}]^{-1} \mathbf{A}^T \bar{\Theta} \\
\mathbf{d} &= [\mathbf{B}^T \mathbf{B}]^{-1} \mathbf{B}^T \bar{\mathbf{w}} - [\mathbf{B}^T \mathbf{B}]^{-1} \mathbf{B}^T \mathbf{C} [\mathbf{A}^T \mathbf{A}]^{-1} \mathbf{A}^T \bar{\Theta} \\
w^* &= [1 \quad x \quad y \quad xy] \mathbf{d} - c_0 \\
w &= [1 \quad x \quad y \quad xy] \mathbf{d} + [x \quad y \quad xy \quad x^2 \quad y^2 \quad x^2 y \quad xy^2] \mathbf{c} \\
w &= [1 \quad x \quad y \quad xy] \left\{ [\mathbf{B}^T \mathbf{B}]^{-1} \mathbf{B}^T \bar{\mathbf{w}} - [\mathbf{B}^T \mathbf{B}]^{-1} \mathbf{B}^T \mathbf{C} [\mathbf{A}^T \mathbf{A}]^{-1} \mathbf{A}^T \bar{\Theta} \right\} \\
&\quad + [x \quad y \quad xy \quad x^2 \quad y^2 \quad x^2 y \quad xy^2] [\mathbf{A}^T \mathbf{A}]^{-1} \mathbf{A}^T \bar{\Theta}
\end{aligned} \quad (\text{C.16})$$

Shear strain can be computed using Eq C.3b

$$\begin{aligned}
\gamma_{xz} &= \frac{\partial w^*}{\partial x} = [0 \quad 1 \quad 0 \quad y] \mathbf{d} \\
\gamma_{yz} &= \frac{\partial w^*}{\partial x} = [0 \quad 0 \quad 1 \quad x] \mathbf{d}
\end{aligned} \quad (\text{C.17})$$

An alternate way of expressing  $w^*$  is, using the conventional isoparametric interpolation functions

$$w^* = \mathbf{N} \bar{\mathbf{w}}^* \quad (\text{C.13a})$$

where  $\bar{\mathbf{w}}^*$  represents values of  $w^*$  at the nodal points. Equation C.14 can be re-written as

$$w = w^* + [x \quad y \quad xy \quad x^2 \quad y^2 \quad x^2 y \quad xy^2] [\mathbf{A}^T \mathbf{A}]^{-1} \mathbf{A}^T \bar{\Theta} \quad (\text{C.14a})$$

$$\bar{\mathbf{w}} = \bar{\mathbf{w}}^* + \mathbf{C} [\mathbf{A}^T \mathbf{A}]^{-1} \mathbf{A}^T \bar{\Theta}$$

and

$$\bar{\mathbf{w}}^* = \bar{\mathbf{w}} - \mathbf{C} [\mathbf{A}^T \mathbf{A}]^{-1} \mathbf{A}^T \bar{\Theta} \quad (\text{C.15a})$$

Then

$$w^* = \mathbf{N} [\bar{\mathbf{w}} - \mathbf{C} [\mathbf{A}^T \mathbf{A}]^{-1} \mathbf{A}^T \bar{\Theta}] \quad (\text{C.16a})$$

$$\begin{aligned}\gamma_{xz} &= \frac{\partial w'}{\partial x} = \frac{\partial N}{\partial x} \left[ \bar{w} - \mathbf{C} [\mathbf{A}^T \mathbf{A}]^{-1} \mathbf{A}^T \bar{\Theta} \right] \\ \gamma_{yz} &= \frac{\partial w'}{\partial y} = \frac{\partial N}{\partial y} \left[ \bar{w} - \mathbf{C} [\mathbf{A}^T \mathbf{A}]^{-1} \mathbf{A}^T \bar{\Theta} \right]\end{aligned}\tag{C.17a}$$

Equation C.17a provides a simpler way of calculating shear strains. The expression inside the brackets contains the nodal deformations but otherwise consists of constants.

### ***Element Family 2***

Calculation of the coefficients in the expression for  $w'$  is done by writing equations which state that at nodal points

$$\begin{aligned}\frac{\partial w'}{\partial y} &= \Theta_x \\ \frac{\partial w'}{\partial x} &= -\Theta_y\end{aligned}\tag{C.18}$$

Thus, each nodal point provides two equations. In Figure C.2, the last two columns show the number of equations available for calculation of coefficients and the number required for Family 1 elements.

For the four-node element, eight equations are available, and there are seven coefficients to be calculated for the Family 1 element. One additional term could be added. Since symmetry is required, the only choice is to add the  $x^2y^2$  term.

Some of the other elements in Figure C.2 offer several choices of additional terms. The six-node triangle allows addition of either one or three terms. The eight-node quadrilateral allows addition of either two or four terms, but there are three possible feasible patterns.

Calculation of element matrices for elements of Family 2 proceeds exactly as for elements of Family 1. There are more terms in  $w'$  defined in Eq. C.5; more columns in Matrix  $\mathbf{A}$ , defined in Eq. C.10; and more unknown coefficients in vector  $\mathbf{c}$ , but the calculation process is otherwise identical.

### ***Out-of-Plane Shear Using Weighted Least Squares***

In the generalized Utku procedure for generating the out-of-plane shear stiffness submatrix, the nodal rotations,  $\bar{\Theta}$ , are related to parameters  $\mathbf{c}$  from the function describing the “Kirchhoffian deflection”,  $w'$ , by

$$\bar{\Theta} = \mathbf{A}\mathbf{c}\tag{C.19}$$

Usually, matrix  $\mathbf{A}$  has more rows than columns, and a least squares solution for  $\mathbf{c}$  is required. This solution can be weighted by introducing a diagonal matrix of weights,  $\mathbf{W}$ . For example, side nodes of a 6-node triangle could be weighted differently from corner nodes.



$$W\bar{\Theta} = WAc \quad [C.20]$$

$$A^T W\bar{\Theta} = A^T WAc$$

$$c = [A^T WA]^{-1} A^T W\bar{\Theta} \quad [C.21]$$

This weighting can be easily introduced by replacing  $A^T$  by  $A^T W$ .

For example, to weight corner nodes differently from side nodes in the 6-node triangle, with rotations order as

$$\bar{\Theta}^T = [\Theta_{x1} \quad \Theta_{y1} \quad \Theta_{x2} \quad \Theta_{y2} \quad \Theta_{x3} \quad \Theta_{y3} \quad \dots] \quad [C.22]$$

Simply multiply the first 6 columns of  $A^T$  by the corner node weight coefficient, which leaves  $W_i = 1$  for side nodes. An extensive numerical study indicates that 0.07 is a good value for corner node weights in 6-node elements.

This treatment of shear strains is strictly valid only for flat elements, but works very well in curved elements if the included angle between outward normals is not too large, as demonstrated by test cases. In the Scordelis-Lo roof it works very well with only two elements, each spanning 40 degrees. However, most performance data is from standard tests where the elements only span about 20 degrees.

## Appendix D

### Strain Calculation at Nodes

Strains are initially calculated at integration points, but values are desired at other locations, especially at nodal points. Strains are derivatives of displacements, and should be interpolated by functions one order lower than displacements.

In the case of the 6-node triangle, displacements vary quadratically, and linear functions are used to interpolate strains. Using 3 integration points, the relation between integration point strains and strains at the 3 corner nodes is

$$\begin{bmatrix} \varepsilon_{p1} \\ \varepsilon_{p2} \\ \varepsilon_{p3} \end{bmatrix} = \begin{bmatrix} N_{1p1} & N_{2p1} & N_{3p1} \\ N_{1p2} & N_{2p2} & N_{3p2} \\ N_{1p3} & N_{2p3} & N_{3p3} \end{bmatrix} \begin{bmatrix} \varepsilon_{N1} \\ \varepsilon_{N2} \\ \varepsilon_{N3} \end{bmatrix} = \begin{bmatrix} \frac{2}{3} & \frac{1}{6} & \frac{1}{6} \\ \frac{1}{6} & \frac{2}{3} & \frac{1}{6} \\ \frac{1}{6} & \frac{1}{6} & \frac{2}{3} \end{bmatrix} \begin{bmatrix} \varepsilon_{N1} \\ \varepsilon_{N2} \\ \varepsilon_{N3} \end{bmatrix} \quad [D1]$$

Or

$$\begin{aligned} \varepsilon_p &= \mathcal{N} \varepsilon_N \\ \varepsilon_N &= \mathcal{N}^{-1} \varepsilon_p \end{aligned} \quad [D2]$$

For 3 components of strain

$$\begin{bmatrix} \varepsilon_{xN1} & \varepsilon_{yN1} & \gamma_{xyN1} \\ \varepsilon_{xN2} & \varepsilon_{yN2} & \gamma_{xyN2} \\ \varepsilon_{xN3} & \varepsilon_{yN3} & \gamma_{xyN3} \end{bmatrix} = \mathcal{N}^{-1} \begin{bmatrix} \varepsilon_{xp1} & \varepsilon_{yp1} & \gamma_{xyp1} \\ \varepsilon_{xp2} & \varepsilon_{yp2} & \gamma_{xyp2} \\ \varepsilon_{xp3} & \varepsilon_{yp3} & \gamma_{xyp3} \end{bmatrix} \quad [D3]$$

Strains at any point can be obtained as

$$\begin{bmatrix} \varepsilon_x & \varepsilon_y & \gamma_{xy} \end{bmatrix} = \begin{bmatrix} N_1 & N_2 & N_3 \end{bmatrix} \begin{bmatrix} \varepsilon_{xN1} & \varepsilon_{yN1} & \gamma_{xyN1} \\ \varepsilon_{xN2} & \varepsilon_{yN2} & \gamma_{xyN2} \\ \varepsilon_{xN3} & \varepsilon_{yN3} & \gamma_{xyN3} \end{bmatrix} = \mathcal{N} \mathcal{N}^{-1} \begin{bmatrix} \varepsilon_{xp1} & \varepsilon_{yp1} & \gamma_{xyp1} \\ \varepsilon_{xp2} & \varepsilon_{yp2} & \gamma_{xyp2} \\ \varepsilon_{xp3} & \varepsilon_{yp3} & \gamma_{xyp3} \end{bmatrix} \quad [D4]$$

or, transposing

$$\begin{bmatrix} \varepsilon_x \\ \varepsilon_y \\ \gamma_{xy} \end{bmatrix} = \begin{bmatrix} \varepsilon_{xp1} & \varepsilon_{xp2} & \varepsilon_{xp3} \\ \varepsilon_{yp1} & \varepsilon_{yp2} & \varepsilon_{yp3} \\ \gamma_{xyp1} & \gamma_{xyp2} & \gamma_{xyp3} \end{bmatrix} \mathcal{N}^{-T} \mathcal{N}^T \quad [D5]$$

This relation can be used to compute strains at any point, including the 6 nodal points. The same process is used for all components of strain; membrane, bending and shear.

### Interlaminar Shear Stresses

Interlaminar shear stresses can be obtained from integration of the equilibrium equations

$$\begin{aligned}\frac{\partial \sigma_x}{\partial x} + \frac{\partial \tau_{xy}}{\partial y} + \frac{\partial \tau_{xz}}{\partial z} &= 0 \\ \frac{\partial \tau_{xy}}{\partial x} + \frac{\partial \sigma_y}{\partial y} + \frac{\partial \tau_{yz}}{\partial z} &= 0 \\ \frac{\partial \tau_{xz}}{\partial x} + \frac{\partial \tau_{yz}}{\partial y} + \frac{\partial \sigma_z}{\partial z} &= 0\end{aligned}\quad [D6]$$

We compute in the local axis

$$\begin{aligned}\tau_{x'z'} &= \int_{-t/2}^{z'} \left( \frac{\partial \sigma_{x'}}{\partial x'} + \frac{\partial \tau_{x'y'}}{\partial y'} \right) dz' \\ \tau_{y'z'} &= \int_{-t/2}^{z'} \left( \frac{\partial \sigma_{y'}}{\partial y'} + \frac{\partial \tau_{x'y'}}{\partial x'} \right) dz'\end{aligned}\quad [D7]$$

$$\begin{bmatrix} \sigma_{x',x'} \\ \sigma_{y',x'} \\ \tau_{x'y',x'} \end{bmatrix} = \mathbf{D} \begin{bmatrix} \varepsilon_{x',x'} \\ \varepsilon_{y',x'} \\ \gamma_{x'y',x'} \end{bmatrix} \quad \text{and} \quad \begin{bmatrix} \sigma_{x',y'} \\ \sigma_{y',y'} \\ \tau_{x'y',y'} \end{bmatrix} = \mathbf{D} \begin{bmatrix} \varepsilon_{x',y'} \\ \varepsilon_{y',y'} \\ \gamma_{x'y',y'} \end{bmatrix}\quad [D8]$$

In Mindlin plates and shells, the strains must vary linearly through the total thickness, and stresses must vary linearly within a layer where material properties are constant.

$$\tau_{x'z'} \Big|_{\text{top of layer } k} = \sum_{i=1}^k \left[ \sigma_{x',x'} + \tau_{x'y',y'} \right]_i t_i \quad [D9]$$

Where  $\sigma_{x',x'}$  and  $\tau_{x'y',y'}$  are average or mid-thickness values in layer  $i$  and  $t_i$  is thickness of layer  $i$ .

Similarly,

$$\tau_{y'z'} \Big|_{\text{top of layer } k} = \sum_{i=1}^k \left[ \sigma_{y',y'} + \tau_{x'y',x'} \right]_i t_i \quad [D10]$$

The ANSYS theoretical manual notes that this summation which starts with  $\tau_{y'z'} = 0$  and  $\tau_{x'z'} = 0$  at the bottom may give  $\tau_{x'z'} \neq 0$  and or  $\tau_{y'z'} \neq 0$  at the top due to inexactness in the calculation. ANSYS has a procedure for distribution this error to make  $\tau_{x'z'} = 0$  at the top, which is also used in our programs.

In the 6-node triangle, which has 3 integration points, strains needed are generated as shown below, and then multiplied by material properties as in Eq [D8] to produce the stresses needed in Eq [D9] and [D10].

$$\begin{bmatrix} \varepsilon_{x',x'} \\ \varepsilon_{y',x'} \\ \gamma_{x'y',x'} \end{bmatrix} = \begin{bmatrix} \varepsilon_{xp1} & \varepsilon_{xp2} & \varepsilon_{xp3} \\ \varepsilon_{yp1} & \varepsilon_{yp2} & \varepsilon_{yp3} \\ \gamma_{xyp1} & \gamma_{xyp2} & \gamma_{xyp3} \end{bmatrix} \mathbf{N}^{-T} \begin{bmatrix} N_{1,x'} \\ N_{2,x'} \\ N_{3,x'} \end{bmatrix} + z \begin{bmatrix} \ominus_{y,x} & \ominus_{y,x} & \ominus_{y,x} \\ -\ominus_{x,y} & -\ominus_{x,y} & -\ominus_{x,y} \\ \ominus_{y,y} - \ominus_{x,x} & \ominus_{y,y} - \ominus_{x,x} & \ominus_{y,y} - \ominus_{x,x} \end{bmatrix} \mathbf{N}^{-T} \begin{bmatrix} N_{1,x'} \\ N_{2,x'} \\ N_{3,x'} \end{bmatrix}$$

$\text{Eval} \int P1 \quad \text{Eval} \int P2 \quad \text{Eval} \int P3$

$$\begin{bmatrix} \varepsilon_{x',y'} \\ \varepsilon_{y',y'} \\ \gamma_{x'y',y'} \end{bmatrix} = \begin{bmatrix} \varepsilon_{xp1} & \varepsilon_{xp2} & \varepsilon_{xp3} \\ \varepsilon_{yp1} & \varepsilon_{yp2} & \varepsilon_{yp3} \\ \gamma_{xyp1} & \gamma_{xyp2} & \gamma_{xyp3} \end{bmatrix} \mathbf{N}^{-T} \begin{bmatrix} N_{1,y'} \\ N_{2,y'} \\ N_{3,y'} \end{bmatrix} + z \begin{bmatrix} \ominus_{y,x} & \ominus_{y,x} & \ominus_{y,x} \\ -\ominus_{x,y} & -\ominus_{x,y} & -\ominus_{x,y} \\ \ominus_{y,y} - \ominus_{x,x} & \ominus_{y,y} - \ominus_{x,x} & \ominus_{y,y} - \ominus_{x,x} \end{bmatrix} \mathbf{N}^{-T} \begin{bmatrix} N_{1,y'} \\ N_{2,y'} \\ N_{3,y'} \end{bmatrix}$$

$\text{Eval} \int P1 \quad \text{Eval} \int P2 \quad \text{Eval} \int P3$

[D11]

In the 6-node triangle, linear interpolation functions for strains,  $N_i$ , are equal to area coordinates  $\xi_i$ , and derivatives in Eq. [D11] are

$$\begin{aligned} N_{1,x'} &= \xi_{1,x'} = l_1 \xi_{,x} + m_1 \xi_{,y} \\ N_{2,x'} &= \xi_{2,x'} = l_1 \eta_{,x} + m_1 \eta_{,y} \\ N_{3,x'} &= \xi_{3,x'} = -l_1 \xi_{,x} - m_1 \xi_{,y} - l_1 \eta_{,x} - m_1 \eta_{,y} \end{aligned}$$

[D12]

$$\begin{aligned} N_{1,y'} &= \xi_{1,y'} = l_2 \xi_{,x} + m_2 \xi_{,y} \\ N_{2,y'} &= \xi_{2,y'} = l_2 \eta_{,x} + m_2 \eta_{,y} \\ N_{3,y'} &= \xi_{3,y'} = -l_2 \xi_{,x} - m_2 \xi_{,y} - l_2 \eta_{,x} - m_2 \eta_{,y} \end{aligned}$$

## Appendix E

### Out-of-Plane Rotation Stiffness

Mindlin plate and shell elements usually have no rotational stiffness associated with the component of the nodal rotation vector that is perpendicular to the element surface. (An exception to this is elements with Allman rotations)

All of our plate/shell element matrices are formulated in element axis with 6 degrees of freedom per node. Two procedures are incorporated which can provide the needed out-of-plane rotational stiffness. Each has a coefficient that can be an input item in the program, to modify the “basic” stiffnesses. The combination of these procedures avoids singularity in flat regions without fixing any degrees of freedom.

Zienkiewicz procedure adds a stiffness to the diagonal of each  $\Theta_z$  degree of freedom, and subtracts  $1/(n-1)$  ( $n$  = number of nodes) of that stiffness from each off-diagonal  $\Theta_z$  degree of freedom in the same row and column. This retains symmetry, equilibrium, and freedom from forces under rigid body motion. Our “basic” stiffness is the average of the nodal in-plane rotational stiffnesses from the bending sub-matrix.

The Kanok Nukulchai procedure is a penalty method which creates an artificial quasi-strain energy,  $U_t$ .

$$U_t = \kappa_t G_{x'y'} t \int \left[ \Theta'_z - \frac{1}{2}(v'_{,x} - u'_{,y}) \right]^2 dA \quad [E1]$$

The quasi-strain,  $\varepsilon_t$ , can be written as

$$\varepsilon_t = \Theta'_z - \frac{1}{2}(v'_{,x} - u'_{,y}) = \mathbf{B}_t \bar{\mathbf{u}} \quad [E2]$$

Where  $\Theta'_z$  ..... local rotation perpendicular to the surface interpolated from nodal values

$\frac{1}{2}(v'_{,x} - u'_{,y})$  ..... elasticity rotation

$G_{x'y'}$  ..... In-surface shear modulus

$t$  ..... thickness

$\kappa_t$  ..... Coefficient for magnitude of stiffness

$\bar{\mathbf{u}}$  ..... vector of nodal displacements

Then, the artificial stiffness matrix is

$$K_t = \kappa_t G_{x'y'} \int \mathbf{B}_t^T \mathbf{B}_t dA = \kappa_t G_{x'y'} \sum_{i=1}^n w_i [\mathbf{B}_i^T \mathbf{B}_i]_i \text{Det} J \quad [E3]$$

Where  $n$  = number of integration points and  $w_i$  = weights.

The determinant of the 3D Jacobian used in our programs is evaluated at the mid-surface.

$$\Theta_z' = [l_3 \quad m_3 \quad n_3] \begin{bmatrix} \Theta_x \\ \Theta_y \\ \Theta_z \end{bmatrix} \quad [\text{E4}]$$

$$\Theta_z' = [N_1(l_3, m_3, n_3) \quad N_2(l_3, m_3, n_3) \quad N_3(l_3, m_3, n_3) \quad N_4(l_3, m_3, n_3)] \begin{bmatrix} \Theta_{x1} \\ \Theta_{y1} \\ \Theta_{z1} \\ \Theta_{x2} \\ \Theta_{y2} \\ \vdots \\ \Theta_{z4} \end{bmatrix} \quad [\text{E5}]$$

For a 4-node element

$$\begin{aligned} u_{,y}' &= u_{,x1}l_2 + v_{,x}m_1l_2 + w_{,x}n_1l_2 \\ &\quad + u_{,y1}m_2 + v_{,y}m_1m_2 + w_{,y}n_1m_2 \\ &\quad + u_{,z}l_2n_2 + v_{,z}m_1n_2 + w_{,z}n_1n_2 \end{aligned} \quad [\text{E6}]$$

$$\begin{aligned} v_{,x}' &= u_{,x}l_2l_1 + v_{,x}m_2l_1 + w_{,x}n_2l_1 \\ &\quad + u_{,y}l_2m_1 + v_{,y}m_2m_1 + w_{,y}n_2m_1 \\ &\quad + u_{,z}l_2n_1 + v_{,z}m_2n_1 + w_{,z}n_2n_1 \end{aligned} \quad [\text{E7}]$$

The derivatives on the right hand side are available from

$$\begin{bmatrix} u_{,x} \\ u_{,y} \\ u_{,z} \\ v_{,x} \\ v_{,y} \\ v_{,z} \\ w_{,x} \\ w_{,y} \\ w_{,z} \end{bmatrix} = \begin{bmatrix} J^{-1} & 0 & 0 \\ 0 & J^{-1} & 0 \\ 0 & 0 & J^{-1} \end{bmatrix} \begin{bmatrix} N_{,\xi} & 0 & 0 \\ N_{,\eta} & 0 & 0 \\ N_{,\zeta} & 0 & 0 \\ 0 & N_{,\xi} & 0 \\ 0 & N_{,\eta} & 0 \\ 0 & N_{,\zeta} & 0 \\ 0 & 0 & N_{,\xi} \\ 0 & 0 & N_{,\eta} \\ 0 & 0 & N_{,\zeta} \end{bmatrix} \begin{bmatrix} \bar{u} \\ \bar{v} \\ \bar{w} \end{bmatrix} \quad [\text{E8}]$$

An extensive numerical study indicates that 1 percent of the average of the in-plane rotational stiffnesses from the bending submatrix is a good value for the Zienkiewicz procedure, and that 0.05 is a good value for the coefficient in the Kanok-Nukulchai procedure.

## Appendix F

### *Simulated Anti-symmetric Bending Mode*

Mindlin elements with 3 or 4 nodes are not capable of anti-symmetric bending, i.e. correct response to linearly varying bending moment. The simulated anti-symmetric bending mode (22, 23, 24) substitutes shear deflection for bending deflection and preserves the correct total strain energy in “beam strips”.

For one layer, a reduced shear modulus,  $G_{xz}^*$ , for a strip in the local  $x$  direction is

$$\frac{1}{G_{xz}^*} = \frac{1}{G_{xz}} + \frac{[\alpha L_x]^2}{E_x h^2} \quad [F1]$$

Where  $L_x$  is the length of the strip,  $E_x$  is the bending modulus, and  $h$  is the thickness (depth) of the strip, and  $\alpha$  is an effective length factor.

For symmetric orthotropic layers

$$\frac{1}{\int_{-h/2}^{h/2} G_{xz}^* dz} = \frac{1}{\int_{-h/2}^{h/2} G_{xz} dz} + \frac{[\alpha L_x]^2}{12 \int_{-h/2}^{h/2} \bar{Q}_{xz} z^2 dz} \quad [F2]$$

For general orthotropic layers

$$\frac{1}{\int_{-h/2}^{h/2} C_{55}^* dz} = \frac{1}{\int_{-h/2}^{h/2} C_{55} dz} + \frac{[\alpha L_x]^2}{12 \Phi} \quad [F3]$$

$$\Phi = \int_{-h/2}^{h/2} \bar{Q}_{11} [\Gamma^2 - 2\Gamma z + z^2] dz$$

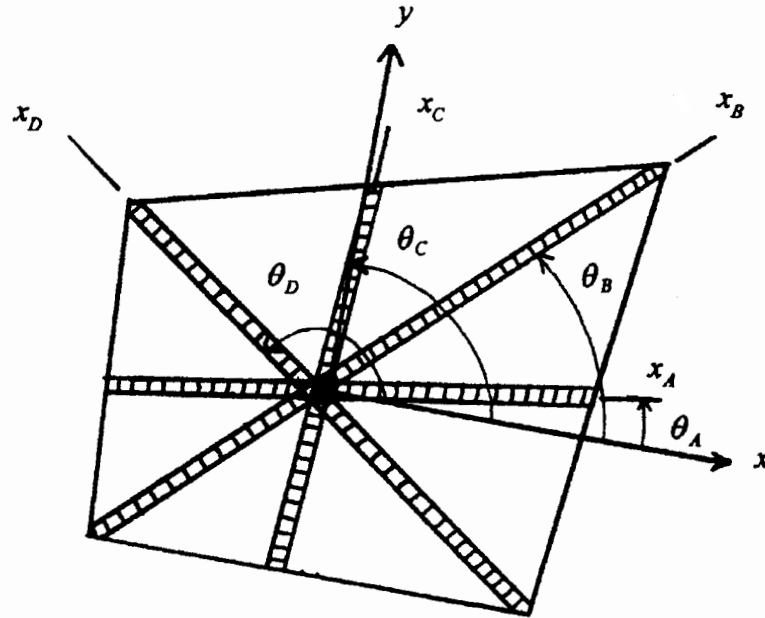
$$\Gamma = \frac{\int_{-h/2}^{h/2} z \bar{Q}_{11} dz}{\int_{-h/2}^{h/2} \bar{Q}_{11} dz}$$

The notation for  $\bar{Q}$  is used as defined by R. M. Jones.



In the local x axis,  $C_{55} = G_{xz}$  and  $\bar{Q}_{11} = E_x$ .

In the four node element, 4 strips are used. The effective length factors,  $\alpha$ , are 0.707 for the diagonal strips and 1.0 for strips connecting midsides.



$$\begin{bmatrix} \int C_{55}^* dz \Big|_A \\ \int C_{55}^* dz \Big|_B \\ \int C_{55}^* dz \Big|_C \\ \int C_{55}^* dz \Big|_D \end{bmatrix} = \begin{bmatrix} \sin^2 \theta_A & 2 \sin \theta_A \cos \theta_A & \cos^2 \theta_A \\ \sin^2 \theta_B & 2 \sin \theta_B \cos \theta_B & \cos^2 \theta_B \\ \sin^2 \theta_C & 2 \sin \theta_C \cos \theta_C & \cos^2 \theta_C \\ \sin^2 \theta_D & 2 \sin \theta_D \cos \theta_D & \cos^2 \theta_D \end{bmatrix} \begin{bmatrix} \int C_{44}^* dz \\ \int C_{45}^* dz \\ \int C_{55}^* dz \end{bmatrix} \quad [F4]$$

Values of  $\int C_{55}^*$  on the left hand side are calculated for each “beam strip”, which requires appropriate material property transformations. The equation above is then solved for by least squares to yield

$$\int C_{44}^* dz, \int C_{45}^* dz, \text{ and } \int C_{55}^* dz$$

in the element axis.

If the shearing stiffness sub-matrix is integrated through the thickness before integration over the area, these integrals are used directly. Otherwise, ratios of reduced integrals to true integrals are computed and these ratios applied to out-of-plane shear moduli.

In the triangular element, strips are taken parallel to each side and the theoretical effective lengths should be  $\alpha = 0.707$ .

This procedure has worked very well in 3-node triangular elements. In 4-node elements it is very good in some deformation modes, such as in a cantilever beam. However, in a centrally loaded square plate modeled by 4-node elements it is too soft, so the coefficients need to be reduced from the theoretical values derived above. More study of this is needed.

## APPENDIX G

### 6-Node Flat Shear Panel (Using 10 Node Shape Functions)

Out-of-plane shear strains can be calculated entirely in curvilinear coordinates, as shown here. Numerical results from this process are identical to those obtained by using a complete cubic polynomial in the procedure of Appendix C. While the development in this Appendix is strictly valid only for a flat shear panel, it is an important step towards development of a curved shear panel. The interpolation functions for a 10-node triangle are used as a convenient representation of a cubic polynomial, and the parameters,  $c_i$ , just happen to correspond to deflections at the nodes of a 10-node triangle.

The total displacement  $w$  from bending and shear is expressed as

$$w = w^* + w^+ \quad [G1]$$

Where  $w^*$  represents shear displacement and  $w^+$  is bending.

Note that

$$w^+ = N_i c_i \quad [G2]$$

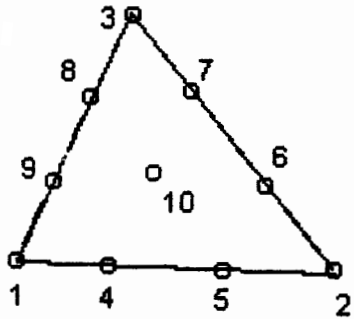


Figure G-1 10-Node Triangle

The functions,  $N_i$ , are

For the corners ( $i=1,2,3$ )

$$N_i = \frac{1}{2} \xi_i (3\xi_i - 1)(3\xi_i - 2)$$

For the mid-side nodes and node 10

$$\begin{aligned}
N_{10} &= 27\xi_1\xi_2\xi_3 \\
N_4 &= \frac{9}{2}\xi_2\xi_1(3\xi_1 - 1) \\
N_5 &= \frac{9}{2}\xi_1\xi_2(3\xi_2 - 1) \\
N_6 &= \frac{9}{2}\xi_3\xi_2(3\xi_2 - 1) \\
N_7 &= \frac{9}{2}\xi_2\xi_3(3\xi_3 - 1) \\
N_8 &= \frac{9}{2}\xi_1\xi_3(3\xi_3 - 1) \\
N_9 &= \frac{9}{2}\xi_3\xi_1(3\xi_1 - 1)
\end{aligned} \tag{G3}$$

We require  $w^+ = N_i c_i$  as a function of  $\xi_1, \xi_2, \xi_3$  and  $c_i$ . This allows us to compute

$$\begin{aligned}
\frac{\partial w^+}{\partial x} &= \frac{\partial N_i}{\partial x} c_i \\
\frac{\partial w^+}{\partial y} &= \frac{\partial N_i}{\partial y} c_i
\end{aligned} \tag{G4}$$

Note

$$\frac{\partial N_i}{\partial x} = \frac{\partial N_i}{\partial \xi} \frac{\partial \xi}{\partial x} + \frac{\partial N_i}{\partial \eta} \frac{\partial \eta}{\partial x} \tag{G5}$$

From Cook

$$\begin{aligned}
\xi_1 &= \xi \\
\xi_2 &= \eta \\
\xi_3 &= 1 - \xi - \eta
\end{aligned} \tag{G6}$$

Which yields

$$\begin{aligned}
\frac{\partial N_i}{\partial \xi} &= \frac{\partial N_i}{\partial \xi_1} - \frac{\partial N_i}{\partial \xi_3} \\
\frac{\partial N_i}{\partial \eta} &= \frac{\partial N_i}{\partial \xi_2} - \frac{\partial N_i}{\partial \xi_3}
\end{aligned} \tag{G7}$$

Finally, the derivatives of the functions  $N$  with respect to  $\xi$  are

$$\begin{aligned}
N_{1,\xi} &= \frac{1}{2}[27\xi_1^2 - 18\xi_1 + 2] \\
N_{2,\xi} &= 0 \\
N_{3,\xi} &= -\frac{1}{2}[27\xi_3^2 - 18\xi_3 + 2] \\
N_{4,\xi} &= \frac{9}{2}[6\xi_1\xi_2 - \xi_2] \\
N_{5,\xi} &= \frac{9}{2}[3\xi_2^2 - \xi_2] \\
N_{6,\xi} &= -\frac{9}{2}[3\xi_2^2 - \xi_2] \\
N_{7,\xi} &= -\frac{9}{2}[\xi_2(3\xi_3 - 1) + 3\xi_2\xi_3] \\
N_{8,\xi} &= \frac{9}{2}[\xi_3(3\xi_3 - 1) - \xi_1(3\xi_3 - 1) - 3\xi_1\xi_3] \\
N_{9,\xi} &= \frac{9}{2}[\xi_3(3\xi_1 - 1) + 3\xi_1\xi_3 - \xi_1(3\xi_1 - 1)] \\
N_{10,\xi} &= 27[\xi_2\xi_3 - \xi_1\xi_2]
\end{aligned}
\tag{G8}$$

and with respect to  $\eta$  as

$$\begin{aligned}
N_{1,\eta} &= 0 \\
N_{2,\eta} &= \frac{1}{2}[27\xi_2^2 - 18\xi_2 + 2] \\
N_{3,\eta} &= -\frac{1}{2}[27\xi_3^2 - 18\xi_3 + 2] \\
N_{4,\eta} &= \frac{9}{2}[3\xi_1^2 - \xi_1] \\
N_{5,\eta} &= \frac{9}{2}[6\xi_1\xi_2 - \xi_1] \\
N_{6,\eta} &= \frac{9}{2}[\xi_3(3\xi_2 - 1) - \xi_2(3\xi_2 - 1) + 3\xi_2\xi_3] \\
N_{7,\eta} &= \frac{9}{2}[\xi_3(3\xi_3 - 1) - \xi_2(3\xi_3 - 1) - 3\xi_2\xi_3] \\
N_{8,\eta} &= -\frac{9}{2}[\xi_1(3\xi_3 - 1) + 3\xi_1\xi_3] \\
N_{9,\eta} &= -\frac{9}{2}[3\xi_1^2 - \xi_1] \\
N_{10,\eta} &= 27[\xi_1\xi_3 - \xi_1\xi_2]
\end{aligned}
\tag{G9}$$

We need  $\frac{\partial \xi}{\partial x}, \frac{\partial \eta}{\partial x}, \frac{\partial \xi}{\partial y}, \frac{\partial \eta}{\partial y}$

Use 6-Node Shape Functions

$$x = N_j \bar{x}_j$$

$$y = N_j \bar{y}_j$$

$$j = 1 \text{ to } 6$$

[G10]

From Cook

$$J = \begin{bmatrix} \frac{\partial x}{\partial \xi} & \frac{\partial y}{\partial \xi} \\ \frac{\partial x}{\partial \eta} & \frac{\partial y}{\partial \eta} \end{bmatrix} = \begin{bmatrix} 4\xi_1 - 1 & 0 & -4\xi_3 + 1 & 4\xi_2 & -4\xi_2 & 4(\xi_3 - \xi_1) \\ 0 & 4\xi_2 - 1 & -4\xi_3 + 1 & 4\xi_1 & 4(\xi_3 - \xi_2) & 4\xi_1 \end{bmatrix} \begin{bmatrix} x_1 & y_1 \\ x_2 & y_2 \\ x_3 & y_3 \\ x_4 & y_4 \\ x_5 & y_5 \\ x_6 & y_6 \end{bmatrix} \quad [\text{G11}]$$

For  $j=1$  to 6

$$\Gamma = J^{-1} = \frac{1}{|J|} \begin{bmatrix} J_{22} & -J_{12} \\ -J_{21} & J_{11} \end{bmatrix} = \frac{1}{\begin{bmatrix} \frac{\partial x}{\partial \xi} & \frac{\partial y}{\partial \xi} \\ \frac{\partial x}{\partial \eta} & \frac{\partial y}{\partial \eta} \end{bmatrix}} \begin{bmatrix} \frac{\partial y}{\partial \eta} & -\frac{\partial y}{\partial \xi} \\ -\frac{\partial x}{\partial \eta} & \frac{\partial x}{\partial \xi} \end{bmatrix} \quad [\text{G12}]$$

$$\Gamma = \begin{bmatrix} \frac{\partial \xi}{\partial x} & \frac{\partial \eta}{\partial x} \\ \frac{\partial \xi}{\partial y} & \frac{\partial \eta}{\partial y} \end{bmatrix} \quad [\text{G13}]$$

Recall from G2

$$w^* = [N_1 \quad N_2 \quad N_3 \quad N_4 \quad N_5 \quad N_6 \quad N_7 \quad N_8 \quad N_9 \quad N_{10}] \begin{bmatrix} c_1 \\ c_2 \\ c_3 \\ c_4 \\ c_5 \\ c_6 \\ c_7 \\ c_8 \\ c_9 \\ c_{10} \end{bmatrix}$$

$$\begin{bmatrix} \theta_{x1} \\ \theta_{y1} \\ \theta_{x2} \\ \theta_{y2} \\ \theta_{x3} \\ \theta_{y3} \\ \theta_{x4} \\ \theta_{y4} \\ \theta_{x5} \\ \theta_{y5} \\ \theta_{x6} \\ \theta_{y6} \end{bmatrix} = \begin{bmatrix} \frac{\partial w^+}{\partial y} \\ \frac{\partial w^+}{\partial x} \\ \frac{\partial w^+}{\partial y} \\ \frac{\partial w^+}{\partial x} \\ \frac{\partial w^+}{\partial y} \\ \frac{\partial w^+}{\partial x} \\ \frac{\partial w^+}{\partial y} \\ \frac{\partial w^+}{\partial x} \\ \frac{\partial w^+}{\partial y} \\ \frac{\partial w^+}{\partial x} \\ \frac{\partial w^+}{\partial y} \\ \frac{\partial w^+}{\partial x} \end{bmatrix} = \begin{bmatrix} \frac{\partial N_1}{\partial y} & \frac{\partial N_2}{\partial y} & \dots & \frac{\partial N_{10}}{\partial y} \\ \frac{\partial N_1}{\partial x} & \frac{\partial N_2}{\partial x} & \dots & \frac{\partial N_{10}}{\partial x} \\ \frac{\partial N_1}{\partial y} & \frac{\partial N_2}{\partial y} & \dots & \frac{\partial N_{10}}{\partial y} \\ \frac{\partial N_1}{\partial x} & \frac{\partial N_2}{\partial x} & \dots & \frac{\partial N_{10}}{\partial x} \\ \frac{\partial N_1}{\partial y} & \frac{\partial N_2}{\partial y} & \dots & \frac{\partial N_{10}}{\partial y} \\ \frac{\partial N_1}{\partial x} & \frac{\partial N_2}{\partial x} & \dots & \frac{\partial N_{10}}{\partial x} \\ \frac{\partial N_1}{\partial y} & \frac{\partial N_2}{\partial y} & \dots & \frac{\partial N_{10}}{\partial y} \\ \frac{\partial N_1}{\partial x} & \frac{\partial N_2}{\partial x} & \dots & \frac{\partial N_{10}}{\partial x} \\ \frac{\partial N_1}{\partial y} & \frac{\partial N_2}{\partial y} & \dots & \frac{\partial N_{10}}{\partial y} \\ \frac{\partial N_1}{\partial x} & \frac{\partial N_2}{\partial x} & \dots & \frac{\partial N_{10}}{\partial x} \\ \frac{\partial N_1}{\partial y} & \frac{\partial N_2}{\partial y} & \dots & \frac{\partial N_{10}}{\partial y} \\ \frac{\partial N_1}{\partial x} & \frac{\partial N_2}{\partial x} & \dots & \frac{\partial N_{10}}{\partial x} \end{bmatrix} \begin{bmatrix} c_1 \\ c_2 \\ c_3 \\ c_4 \\ c_5 \\ c_6 \\ c_7 \\ c_8 \\ c_9 \\ c_{10} \end{bmatrix} \tag{G14}$$

Or

$$[\bar{\theta}] = [A][c] \tag{G15}$$

Which allows us to solve for c as

$$[c] = [A^T A]^{-1} A^T [\bar{\theta}] \tag{G16}$$

Note: we generate matrix A in 2-row blocks

For node j

$$\begin{bmatrix} \theta_{xj} \\ \theta_{yj} \end{bmatrix} = \frac{\partial w^+}{\partial \xi} \frac{\partial \xi}{\partial y} + \frac{\partial w^+}{\partial \eta} \frac{\partial \eta}{\partial y} = \begin{bmatrix} \frac{\partial \xi}{\partial y} & \frac{\partial \eta}{\partial y} \\ \frac{\partial \xi}{\partial x} & \frac{\partial \eta}{\partial x} \end{bmatrix} \begin{bmatrix} \frac{\partial N_1}{\partial \xi} & \frac{\partial N_2}{\partial \xi} & \dots & \frac{\partial N_{10}}{\partial \xi} \\ \frac{\partial N_1}{\partial \eta} & \frac{\partial N_2}{\partial \eta} & \dots & \frac{\partial N_{10}}{\partial \eta} \end{bmatrix} \begin{bmatrix} c_1 \\ c_2 \\ \vdots \\ c_{10} \end{bmatrix} \tag{G17}$$

The matrix  $A^T A$  in equation G16 is initially singular. The singularity can be removed by augmenting matrix  $A$  with an equation that assigns a zero value to  $w^+$  at the centroid of the element. After some manipulation, the only change is to add one (1) to  $A^T A_{10,10}$  which removes the singularity and allows inversion.

The terms

$$\begin{bmatrix} \frac{\partial \xi}{\partial y} & \frac{\partial \eta}{\partial y} \\ \frac{\partial \xi}{\partial x} & \frac{\partial \eta}{\partial x} \end{bmatrix}$$

in equation G17 can be obtained from the  $\Gamma$  in equation G13 defined earlier.

Recall G1

$$w = \bar{w}^* + w^+$$

Which we can rewrite as

$$w = N\bar{w}^* + [N_1 \quad N_2 \quad \dots \quad N_{10}] [A^T A]^{-1} A^T \begin{bmatrix} \theta_{x1} \\ \theta_{y1} \\ \vdots \\ \theta_{x6} \\ \theta_{y6} \end{bmatrix} \quad [\text{G18}]$$

This equation must be true at each node so

$$\bar{w} = \bar{w}^* + \begin{bmatrix} N_1 & \text{evaluated at node 1} \\ N_1 & \text{evaluated at node 2} \\ N_1 & \text{evaluated at node 3} \\ \vdots & \vdots \\ N_1 & \text{evaluated at node 10} \end{bmatrix} [A^T A]^{-1} A^T \begin{bmatrix} \theta_{x1} \\ \theta_{y1} \\ \vdots \\ \theta_{x6} \\ \theta_{y6} \end{bmatrix} \quad [\text{G19}]$$

Which can be written more compactly as

$$\bar{w} = \bar{w}^* + X [A^T A]^{-1} A^T [\bar{\theta}] \quad [\text{G20}]$$

This can be rewritten as

$$\bar{w}^* = \bar{w} - X [A^T A]^{-1} A^T [\bar{\theta}] \quad [\text{G21}]$$

Finally, from basic mechanics we may write



$$\begin{bmatrix} \gamma_{xz} \\ \gamma_{yz} \end{bmatrix} = \begin{bmatrix} \frac{\partial w^*}{\partial x} \\ \frac{\partial w^*}{\partial y} \end{bmatrix} = \begin{bmatrix} \frac{\partial N}{\partial x} \\ \frac{\partial N}{\partial y} \end{bmatrix} \bar{w}^* = \begin{bmatrix} \frac{\partial N}{\partial x} \\ \frac{\partial N}{\partial y} \end{bmatrix} [I - X[A^T A]^{-1} A^T] \begin{bmatrix} \bar{w} \\ \bar{\theta} \end{bmatrix} \quad [G22]$$

Where

$$\begin{bmatrix} \frac{\partial N}{\partial x} \\ \frac{\partial N}{\partial y} \end{bmatrix} = \begin{bmatrix} \frac{\partial \xi}{\partial x} & \frac{\partial \eta}{\partial x} \\ \frac{\partial \xi}{\partial y} & \frac{\partial \eta}{\partial y} \end{bmatrix} \begin{bmatrix} 4\xi_1 - 1 & 0 & -4\xi_3 + 1 & 4\xi_2 & -4\xi_2 & 4(\xi_3 - \xi_1) \\ 0 & 4\xi_2 - 1 & -4\xi_3 - 1 & 4\xi_1 & 4(\xi_3 - \xi_2) & 4\xi_1 \end{bmatrix}$$

Applying to the 6-Node flat shear panel yields

$$\begin{bmatrix} \gamma_{xz} \\ \gamma_{yz} \end{bmatrix} = J^{-1} \begin{bmatrix} 4\xi_1 - 1 & 0 & -4\xi_3 + 1 & 4\xi_2 & -4\xi_2 & 4(\xi_3 - \xi_1) \\ 0 & 4\xi_2 - 1 & -4\xi_3 - 1 & 4\xi_1 & 4(\xi_3 - \xi_2) & -4\xi_1 \end{bmatrix} \begin{bmatrix} I & -\Omega[A^T A]^{-1} A^T \end{bmatrix} \begin{bmatrix} \bar{w} \\ \bar{\theta}_{x1} \\ \bar{\theta}_{y1} \\ \vdots \\ \bar{\theta}_{x6} \\ \bar{\theta}_{y6} \end{bmatrix}$$

Where

$$\Omega = \begin{bmatrix} 1 & 0 & 0 & 0 & 0 & 0 & 0 & 0 & 0 & 0 \\ 0 & 1 & 0 & 0 & 0 & 0 & 0 & 0 & 0 & 0 \\ 0 & 0 & 1 & 0 & 0 & 0 & 0 & 0 & 0 & 0 \\ -\frac{1}{16} & -\frac{1}{16} & 0 & \frac{9}{16} & \frac{9}{16} & 0 & 0 & 0 & 0 & 0 \\ 0 & -\frac{1}{16} & -\frac{1}{16} & 0 & 0 & \frac{9}{16} & \frac{9}{16} & 0 & 0 & 0 \\ -\frac{1}{16} & 0 & -\frac{1}{16} & 0 & 0 & 0 & 0 & \frac{9}{16} & \frac{9}{16} & 0 \end{bmatrix}$$

# REPORT DOCUMENTATION PAGE

Form Approved  
OMB No. 0704-0188

Public reporting burden for this collection of information is estimated to average 1 hour per response, including the time for reviewing instructions, searching existing data sources, gathering and maintaining the data needed, and completing and reviewing the collection of information. Send comments regarding this burden estimate or any other aspect of this collection of information, including suggestions for reducing this burden, to Washington Headquarters Services, Directorate for Information Operations and Reports, 1215 Jefferson Davis Highway, Suite 1204, Arlington, VA 22202-4302, and to the Office of Management and Budget, Paperwork Reduction Project (0704-0188), Washington, DC 20503.

<b>1. AGENCY USE ONLY (Leave blank)</b>	<b>2. REPORT DATE</b> July 2004	<b>3. REPORT TYPE AND DATES COVERED</b> Contractor Report	
<b>4. TITLE AND SUBTITLE</b> A Six-Node Curved Triangular Element and a Four-Node Quadrilateral Element for Analysis of Laminated Composite Aerospace Structures			<b>5. FUNDING NUMBERS</b>  710-55-24-E8-RR-00-000
<b>6. AUTHOR(S)</b> C. Wayne Martin and David M. Breiner			
<b>7. PERFORMING ORGANIZATION NAME(S) AND ADDRESS(ES)</b> NASA Dryden Flight Research Center P.O. Box 273 Edwards, California 93523-0273			<b>8. PERFORMING ORGANIZATION REPORT NUMBER</b>  H-2469
<b>9. SPONSORING/MONITORING AGENCY NAME(S) AND ADDRESS(ES)</b> National Aeronautics and Space Administration Washington, DC 20546-0001			<b>10. SPONSORING/MONITORING AGENCY REPORT NUMBER</b>  NASA/CR-2004-210725
<b>11. SUPPLEMENTARY NOTES</b> This work was done as partial fulfillment for contract numbers NAS4-97007, NAS4-50079, NCA2-318, and NCA2-497 ranging from 1991-1998. NASA Technical Monitor – Kajal K. Gupta, NASA Dryden Flight Research Center.			
<b>12a. DISTRIBUTION/AVAILABILITY STATEMENT</b>  Unclassified—Unlimited Subject Category 05  This report is available at <a href="http://www.dfrc.nasa.gov/DTRS/">http://www.dfrc.nasa.gov/DTRS/</a>			<b>12b. DISTRIBUTION CODE</b>
<b>13. ABSTRACT (Maximum 200 words)</b>  Mathematical development and some computed results are presented for Mindlin plate and shell elements, suitable for analysis of laminated composite and sandwich structures. These elements use the conventional 3 (plate) or 5 (shell) nodal degrees of freedom, have no communicable mechanisms, have no spurious shear energy (no shear locking), have no spurious membrane energy (no membrane locking) and do not require arbitrary reduction of out-of-plane shear moduli or under-integration. Artificial out-of-plane rotational stiffnesses are added at the element level to avoid convergence problems or singularity due to flat spots in shells. This report discusses a 6-node curved triangular element and a 4-node quadrilateral element. Findings show that in regular rectangular meshes, the Martin-Breiner 6-node triangular curved shell (MB6) is approximately equivalent to the conventional 8-node quadrilateral with $2 \times 2$ integration. The 4-node quadrilateral (MB4) has very good accuracy for a 4-node element, and may be preferred in vibration analysis because of narrower bandwidth. The mathematical developments used in these elements, those discussed in the seven appendices, have been applied to elements with 3, 4, 6, and 10 nodes and can be applied to other nodal configurations.			
<b>14. SUBJECT TERMS</b>  Aerospace engineering, Composites, Curved elements, Finite element, Structural design			<b>15. NUMBER OF PAGES</b> 58
			<b>16. PRICE CODE</b>
<b>17. SECURITY CLASSIFICATION OF REPORT</b> Unclassified	<b>18. SECURITY CLASSIFICATION OF THIS PAGE</b> Unclassified	<b>19. SECURITY CLASSIFICATION OF ABSTRACT</b> Unclassified	<b>20. LIMITATION OF ABSTRACT</b> Unlimited